UNIVERSIDADE
BEIRA INTERIOR

Produção de um novo substituto para a regeneração da pele

Mariana Filipa Pais Graça

Dissertação para obtenção do Grau de Mestre em
Bioquímica
(2º ciclo de estudos)

Orientador: Professor Doutor Ilídio Joaquim Sobreira Correia
Co-orientador: Doutora Sónia Alexandra Pereira Miguel
Co-orientador: Mestre Cátia Solange Duarte Cabral

junho de 2020

"A grande conquista é o resultado de pequenas vitórias que passam despercebidas."

Paulo Coelho

Para os meus eternos suportes: avós, pais e irmãos

Agradecimentos

A duração da tese é de apenas um ano mas no entanto, no decorrer deste espaço temporal, existiram pessoas que foram essenciais para a entrega desta dissertação ocorrer e às quais quero agradecer.

Em primeiro lugar, quero agradecer ao professor Ilídio Correia por me ter aceite e por toda a sua orientação no decorrer deste ano. Agradeço ainda a sua exigência com todos os alunos, tendo sido esta essencial para o meu crescimento e evolução durante a realização deste trabalho.

À Doutora Sónia Miguel e à Mestre Cátia Cabral, que foram as minhas co-orientadoras, por todo o apoio que me deram durante todos os dias deste ano. Devo em parte a elas a realização deste trabalho, por me ensinarem, aturarem, apoiarem e ainda, por não me deixarem desistir e baixar os braços mesmo quando tudo parecia dar mal. Agradeço-lhes o seu enorme esforço que eu nunca irei esquecerei. Não existem palavras que permitam expressar esse agradecimento.

Agradeço também ao André e ao Duarte pela sua disponibilidade para ajudar os alunos mais novos do grupo, assim como pela motivação emanada por eles e ainda pela sua boa disposição.

Aos meus colegas de grupo, tanto às "frozens" como aos "minis", agradeço pelo acompanhamento diário, tanto a nível de trabalho, como nos momentos de relaxamento e diversão, tendo eles contribuído para que este ano fosse mais fácil e melhor.

Aos amigos próximos que a Covilhã me deu, agradeço pela paciência, apoio, preocupação e persistência que tiveram para comigo, durante todos estes anos. Em especial, gostaria de agradecer às "turbinadas" que apesar de já estar cada uma no seu canto, tornaram todo este trabalho possível com todo o seu apoio e suporte, apesar da distância física que nos separa. Aos amigos da minha cidade natal, em especial, Rafael, Diana e Inês, agradeço o seu incansável apoio e pelo ensinamento em como a distância não é tudo, e que tudo é possível e perdura, apesar disso.

À minha família, avós, pais e irmãos, não existem palavras para vos agradecer. Vocês são o meu maior suporte, melhor porto de abrigo e melhor colo aconchegante. Apesar da distância, não existe maior força, maior amor, maior confiança ou maior orgulho. Todos os dias agradeço a confiança que depositam em mim e tomo-os como exemplo sempre. Agradeço ainda, em especial, à minha irmã por me ter tornado na tia mais babada deste mundo, e à qual prometo eterna proteção às minhas pequenas.

Por fim, agradeço ao meu namorado e acima de tudo, amigo. Agradeço-lhe pela paciência diária quando eu estava de mau feitio por as coisas me correrem mal, pelo apoio quando

eu desmotivava, pela alegria e pelo amor diário. Tenho ainda de agradecer à família dele por me receberem quando mais precisava e facilitarem todos os momentos, tanto os mais difíceis como os mais felizes.

A todos devo um enorme obrigada, por assistirem em primeira fila a todo este crescimento, até ao último dia desta aventura. Só me resta dizer: até à próxima etapa!

Resumo

A pele é o maior e mais externo órgão do corpo humano, que está exposto a diferentes agentes externos que podem causar danos estruturais e funcionais. Apesar da pele ter capacidade de auto-regeneração, esta função fica comprometida quando lesões que afectam este órgão são extensas e profundas. Nestas situações, é necessário o uso de um revestimento que permita proteger a lesão e que promova o processo de cicatrização. Diferentes tipos de revestimentos cutâneos foram já desenvolvidos, contudo, nenhum deles é capaz de restaurar na íntegra todas as funções estruturais e funcionais da pele nativa. Assim, os investigadores da área de engenharia de tecidos têm desenvolvido novos substitutos de pele que sejam capazes de reproduzir a estrutura e composição da pele nativa. Entre os substitutos de pele produzidos até ao momento, as membranas assimétricas têm revelado resultados promissores no tratamento de lesões da pele. Neste estudo, o plano de trabalhos desenvolvido teve como objetivo a produção de uma membrana assimétrica pela técnica de electrofiação e a posterior caracterização das suas propriedades fisico-químicas e biológicas. Na produção das duas camadas da membrana assimétrica foram usados diferentes materiais. A policaprolactona e o acetato de celulose foram usados na produção da camada superior. Esta camada, à semelhança da epiderme na pele nativa, pretende-se que actue como uma barreira de proteção. Por outro lado, a camada inferior da membrana assimétrica foi produzida com poli(álcool polivinílico) e ácido hialurónico com o intuito de mimetizar as características da derme (*i.e.,* elevada porosidade e capacidade de absorção). Neste trabalho foram ainda produzidas e caracterizadas nanopartículas de prata com o objectivo de incrementar as suas propriedades antibacterianas. Os resultados obtidos neste estudo revelaram que as membranas produzidas têm uma porosidade adequada que permite a troca de gases e a migração celular, a absorção do exsudato da ferida e providenciam um ambiente húmido ao local da lesão. Para além disso, os ensaios *in vitro* demonstraram que as membranas produzidas apresentam excelente biocompatibilidade em contacto com fibroblastos humanos. Por outro lado, as nanopartículas de prata produzidas possuem tamanho, morfologia e propriedades antibacterianas promissoras para a prevenção de infeções. Assim, no futuro, a incorporação das nanopartículas de prata na membrana inferior será realizada de modo a providenciar propriedades antibacterianas à membrana assimétrica. Por outro lado, a incorporação de outras moléculas bioativas (vitaminas, fatores de crescimento, moléculas anti-inflamatórias) poderá também ser realizada a fim de melhorar as propriedades biológicas da membrana assimétrica e, consequentemente o processo de cicatrização.

Palavras-chave

Membranas eletrofiadas; membranas assimétricas; atividade antibacteriana; nanopartículas de prata; revestimento cutâneo; regeneração da pele

Resumo alargado

A pele é o maior e mais extenso órgão do corpo humano, com 2 m^2 de área e 2,5 mm de espessura. Este órgão desempenha diferentes funções importantes no organismo humano, tais como, a termorregulação, prevenção de perda de água e fluidos, deteção sensorial, vigilância imunológica e síntese hormonal. Para além disto, a pele atua também como uma barreira protetora contra a invasão microbiana e radiação UV. Anatomicamente, a pele é constituída essencialmente por três camadas: a epiderme, a derme e a hipoderme.

Diariamente, a pele encontra-se exposta a diferentes agentes que podem causar lesões, o que despoleta imediatamente o processo de cicatrização com o objetivo de restaurar a estrutura e funções nativas da pele, bem como evitar a ocorrência de infeções.

Atualmente, o uso de enxertos (autoenxertos, aloenxertos e xenoenxertos) continua a ser a terapia mais usada no meio clínico para o tratamento de feridas. Apesar das vantagens apresentadas pelos enxertos, estes apresentam uma disponibilidade limitada, risco elevado de infeções e rejeição imunológica. Assim, os investigadores da área de engenharia de tecidos têm vindo a desenvolver diferentes substitutos cutâneos (filmes, hidrogéis, hidrocolóides), com o intuito de melhorar e acelerar o processo de cicatrização de feridas. No entanto, estes apresentam algumas desvantagens, como a adesão à superfície da lesão, possibilidade de induzir a maceração do tecido lesado, reposição periódica e, até ao momento, nenhum restaura na íntegra a estrutura e funções nativas da pele.

Entre os diferentes substitutos de pele desenvolvidos, as membranas assimétricas têm revelado propriedades promissoras para a sua utilização no tratamento de lesões da pele. Estes sistemas são caracterizados por possuírem duas camadas com propriedades e funções distintas, o que lhes permite mimetizar as duas camadas da pele nativa, *i.e.,* epiderme e derme. Para além disso, a sua elevada área de superfície permite promover uma maior capacidade de absorção, assim como promover a adesão celular. Este tipo de membranas apresenta também uma elevada porosidade que lhes permite efectuar trocas gasosas, suprimento de nutrientes, controlo de perda de fluidos e conferir proteção contra infeções. Quando colocadas sobre uma ferida, estas membranas conferem um ambiente húmido no local da lesão, o que proporciona uma maior migração, adesão, proliferação e diferenciação celular.

Processos como a auto-montagem, separação de fases e eletrofiação têm sido usados na produção destas membranas. Contudo, a técnica de eletrofiação tem sido a mais utilizada

devido à sua simplicidade, versatilidade e possibilidade de utilizar diferentes polímeros na produção das membranas.

Considerando isto, o trabalho desenvolvido durante o meu mestrado, teve como objetivo a produção por electrofiação de uma membrana assimétrica que reproduza as duas camadas existentes na pele nativa. A caracterização das membranas produzidas revelou que a camada superior, composta por policaprolactona e acetato de celulose, é biocompatível e tem um caracter hidrofóbico adequado à sua utilização na aplicação biomédica pretendida. Por outro lado, a camada inferior da membrana, produzida com poli(álcool polivinílico) e ácido hialurónico, é biodegradável e hidrofílica, estimulando a migração, adesão e proliferação celular. Foram ainda sintetizadas e caracterizadas nanopartículas de prata, como agente antimicrobiano.

Os resultados obtidos no presente estudo revelam que a porosidade e capacidade de absorção de líquidos que as membranas produzidas apresentam, permite a estes dispositivos conferir um ambiente húmido no local da ferida, ambiente este que estimula a adesão e proliferação celular. Por outro lado, os ensaios *in vitro* demonstraram a biocompatibilidade das membranas assimétricas aqui produzidas, uma vez que as mesmas não induziram nenhum efeito citotóxico nos fibroblastos humanos. Por outro lado, as nanopartículas de prata produzidas possuem tamanho, morfologia e propriedades antibacterianas promissoras para a prevenção de infeções. Deste modo, as propriedades apresentadas pelas membranas assimétricas produzidas são adequadas para o uso no tratamento de lesões cutâneas. No futuro, a incorporação das nanopartículas de prata na membrana inferior, será realizada a fim de providenciar propriedades antibacterianas à membrana assimétrica. Por outro lado, a incorporação de outras moléculas bioativas (vitaminas, fatores de crescimento, moléculas anti-inflamatórias) poderá também ser realizada a fim de melhorar as propriedades biológicas da membrana assimétrica e, consequentemente o processo de cicatrização.

Abstract

The skin is the largest and most external organ of the human body, and it is exposed to different external agents that may cause structural and functional damage. Despite skin's self-regeneration ability, skin structure can be compromised when extensive and deep injuries occur. In these situations, wound dressings capable of protecting the lesion as well as promote the healing process are required. So far, different types of skin substitutes have been developed. However, none of them is fully capable of re-establishing all the structural and functional features of the native skin. To overcome this situation, researchers from the tissue engineering area have been developing new biomaterials that are capable of reproducing the structure and composition of native skin. In this way, asymmetric membranes emerged as promising therapeutic approaches for the treatment of skin lesions, since they display two layers with different properties and functions. The work plan developed herein aimed to produce asymmetric membranes, using electrospinning technique, that are able to mimic both layers of the native skin. Therefore, the top membrane was manufactured with polycaprolactone and cellulose acetate, in order to act as the epidermis layer of the membrane. On the other hand, the bottom layer of the membrane was produced with poly (vinyl alcohol) and hyaluronic acid to replicate the characteristics of the dermis (high porosity and absorption capacity). In additon, silver nanoparticles were also produced to confer antimicrobial properties to the membranes. The characterization of the physicochemical properties of the produced membranes revealed that they have a porosity and water absorption capacity that provides a moist environment to the wound site. On the other side, the *in vitro* assays showed that the produced membranes did not induce any cytotoxic effect, when they were incubated in contact with human fibroblasts cells. Further, the silver nanoparticles possess suitable size, morphology and antibacterial properties for preventing infections. In this way, the produced membranes showed promising properties to be used in the treatment of skin lesions. Thus, in the future, the incorporation of silver nanoparticles into the bottom membrane will be performed to provide antibacterial properties to the asymmetric membrane. On the other side, the incorporation of other bioactive molecules (vitamins, growth factors, anti-inflammatory molecules) could also be hypothesized to augment the biological performance of the asymmetric membrane and consequently, the wound healing process.

Keywords

Electrospun membranes, Asymmetric membranes, Antibacterial activity, Silver nanoparticles, Wound dressing; Skin regeneration

List of Publications

Articles published in international peer reviewed journals:

Mariana F.P. Graça, Sónia P. Miguel, Cátia S. D. Cabral, Ilídio J. Correia. (2020). Hyaluronic acid-based wound dressings: a review. *Carbohydrate Polymers*, **241**: 116364. (DOI: 10.1016/j.carbpol.2020.116364).

Contents

Chapter I – Introduction

Chapter II - Materials and Methods

Chapter III - Results and Discussion

Chapter IV - Conclusion and Future Perspectives

Chapter V - References

List of Figures

Chapter I - Introduction

Chapter III - Results and Discussion

List of tables

Chapter I – Introduction

Chapter III - Results and Discussion

Acronyms

3D	Three-dimensional
AgNPs	Silver nanoparticles
ATR-FTIR	Attenuated total reflectance-Fourier transform infrared spectroscopy
bFGF	Basic fibroblast growth factor
BM	Bilayer membrane
CA	Cellulose acetate
CFU	Colony-forming units
ChS	Chitosan sponge
CS	Chitosan
CSGT	Chitosan-gelatin sponge crosslinked with tannin acid
DMEM-F12	Dulbecco's modified eagle's medium
DLS	Dynamic light scattering
E. coli	*Escherichia coli*
ECM	Extracellular matrix
EDTA	Ethylenediaminetetraacetic acid
FBS	Fetal bovine serum
Gel	Gelatin
GF	Growth factors
GS	Gelatin sponge
HA	Hyaluronic acid
IFN-γ	Interferon-γ
IL-1β	Interleukin-1β
Law	Lawsone
MIC	Minimum inhibitory concentration
MTS	3-(4,5-dimethylthiazol- 2-yl)-5-(3-carboxymethoxyphenyl)-2 (4-sulfophenyl)-2H-tetrazolium salt
NHDF	Normal human dermal fibroblasts
P. aeruginosa	*Pseudomonas aeruginosa*
PBS	Phosphate-buffered saline solution
PCL	Poly(caprolactone)
PDGF	Platelet-derived growth factor
PDLLA	Poly(D,L-lactic acid)
PEO	Poly(ethylene oxide)
PLA	Polylactic acid

PLGA	Poly(lactide-co-glycolide)
PMS	Phenazine methosulfate
PRP	Platelet-rich plasma
PU	Polyurethane
PVA	Poly(vinyl alcohol)
PVP	Polyvinylpyrrolidone
ROS	Reactive oxygen species
RT	Room temperature
S. aureus	*Staphylococcus aureus*
SA	Salicylic acid
SEM	Scanning electron microscopy
SF	Silk fibroin
SPG	Schizophyllan
TEM	Transmission electron microscopy
TGF-β	Transforming growth factor-β
THY	Thymol
TNF-α	Tumor necrosis factor-α
Tris-HCL	Tris hydrochloride
VEGF	Vascular endothelial growth factor
WCA	Water contact angle
WVTR	Water vapor transmission rate
ZN	Zein

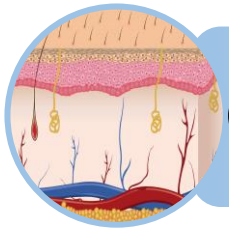

Chapter I - Introduction

1.Introduction

1.1. Skin structure and functions

Skin is the largest and outermost organ of the human body, with 2 m^2 of area and 2.5 mm of thick, it is integrated into the underlying fascial endoskeleton through retinacular ligaments, blood vessels and nerves [1, 2]. Such organ plays several important functions in the human body, namely thermoregulation, prevention of water and fluid loss, immune surveillance, hormone synthesis, and sensory detection (due to the presence of sensory nerve receptors) [1, 3]. In addition, it also acts as a barrier against microbial invasion and UV radiation, thus conferring protection to the body [3]. At morphological level, skin is composed of three layers: epidermis, dermis and hypodermis, as well as some appendages, nerves and blood vessels (see further details in Figure 1).

1.1.1. Epidermis

Epidermis is the most superficial layer of the skin and it is located at a depth of 75-150 μm [2]. The keratinocytes (95%) are the most abundant cell type available in epidermis, and they are involved in the prevention of the pathogens invasion during the inflammatory phase as well as participate in the wound contraction process [4]. These cells are able to undergo self-renewal through a continuous process of proliferation, differentiation and cell death.

This continuous keratinocytes differentiation process enables the division of the epidermis into five different layers: the *stratum basale*, *stratum spinosum*, *stratum granulosum*, *stratum lucidum* and *stratum corneum* (from the deepest to the most superficial layer) [5].

The *stratum basale*, which is the deepest portion of the epidermis, is composed of basal cells that proliferate and differentiate into keratinocytes. Then, keratinocytes migrate to the subsequent layer, *stratum spinosum*. In this layer, the keratinocytes are linked through desmosomes, like spinous cells, and the keratinization process begins (production of keratin). At this stage, the keratinocytes suffer shape alteration, lose their cytoplasm and start to synthesize keratin. Then, the differentiated keratinocytes migrate to the *stratum granulosum*, where they accumulate lipid granules, that are essential for the maintenance of a water barrier. In the *stratum lucidum* and *corneum*, cells enter into the programmed cell death process and their cytoplasmic organelles suffer degradation. The *stratum corneum* is the most external layer of the epidermis, and it represents the

final stage of keratinocyte differentiation. This layer is composed of differentiated dead keratinocytes interspersed with intercellular lipids (mainly ceramides and sphingolipids). The keratinized *stratum corneum* is in direct contact with the environment, providing a barrier that is responsible for controlling the water loss as well as avoiding the entrance of pathogens into the body [5, 6].

The epidermis layer is also composed of Langerhans that are involved in skin immune defense system, Merkel cells that act as mechanosensory receptors and melanocytes responsible for the production of melanin, which confers skin color [6, 7].

Furthermore, the epidermis is connected to the dermis through the basement membrane, which are constituted by two layers (the lamina lucida and the lamina dense). The lamina lucida is the layer that is more close to the epidermis and is composed of laminin, integrins, entactins, and dystroglycans. On the other side, the lamina dense is mainly composed of type IV collagen [5].

1.1.2. Dermis

Below the epidermis is found the dermis, a layer that has 2-4 mm of thick, that provides structural as well as nutritional support to the overlying epidermis. Dermis is composed of extracellular matrix (ECM), fibroblasts, vascular endothelial cells, hair follicles, sweat and sebaceous glands, blood vessels and nerve endings [1, 2].

The ECM comprises different macromolecules (collagens, elastin, proteoglycans, hyaluronic acid (HA), fibronectin and laminins), growth factors (GF), cytokines, chemokines, matrix-degrading enzymes, and their inhibitors. Collagens are the most abundant proteins in the ECM and they are responsible for conferring structural support and resistance to skin. The characteristic elasticity displayed by skin is provided by elastin. On the other hand, proteoglycans and HA are involved in the formation of pericellular matrix and tissue homeostasis, as well as in dermis repair, scar formation, and ECM remodelling. Moreover, fibronectin is involved in the ECM-cell signalling, while laminins are able to modulate cell adhesion, differentiation and migration [7, 8].

In terms of cell composition of dermis, the fibroblasts are the most abundant type of cells, that play a crucial role in the wound healing process, since they are involved in the production of collagen and elastin [1, 7].

Furthermore, dermis is divided into two layers: the papillary and the reticular. The papillary dermis, below the dermal-epidermal junction, has a larger surface available for cell attachment, exhibits a greater resistance to shear forces and it is also enrolled in the supply of nutrients to the epidermis. This layer of the dermis is composed of fibrocytes, collagen, elastin, sensorial nerves and blood vessels [2, 6, 9]. In turn, the reticular dermis

is thicker and it is composed of a lower number of fibrocytes, collagen and elastin fibers with a larger diameter, that confer elasticity and flexibility to the skin [2, 6].

1.1.3. Hypodermis

The hypodermis is the bottom layer of the skin and it is mainly composed of adipocytes, blood vessels and inflammatory cells [1]. Furthermore, the hypodermis also possess proteoglycans and glycosaminoglycans in its composition, which gives to this layer mucous-like properties [2]. Hypodermis is responsible for connecting the dermis with the skeletal components as well as the thermoregulation and mechanical protection of the body [10].

1.1.4. Skin appendages

Skin contains several appendages such as hair follicles, nails, sebaceous and sweat glands [11]. The hair follicles with the sebaceous glands are involved in the maintenance of body temperature and sensation [6, 12]. In addition, sebaceous glands secrete sebum rich in lipids, which is a lubricant for the skin and confer antibacterial protection. In turn, nails provide protection to the fingertips and enhance sensibility [11, 12]. Furthermore, the sweat glands regulate body temperature through sweat, which contains free fatty acids and antimicrobial peptides, that are enrolled in the prevention of the microbial colonization of the skin [10, 13].

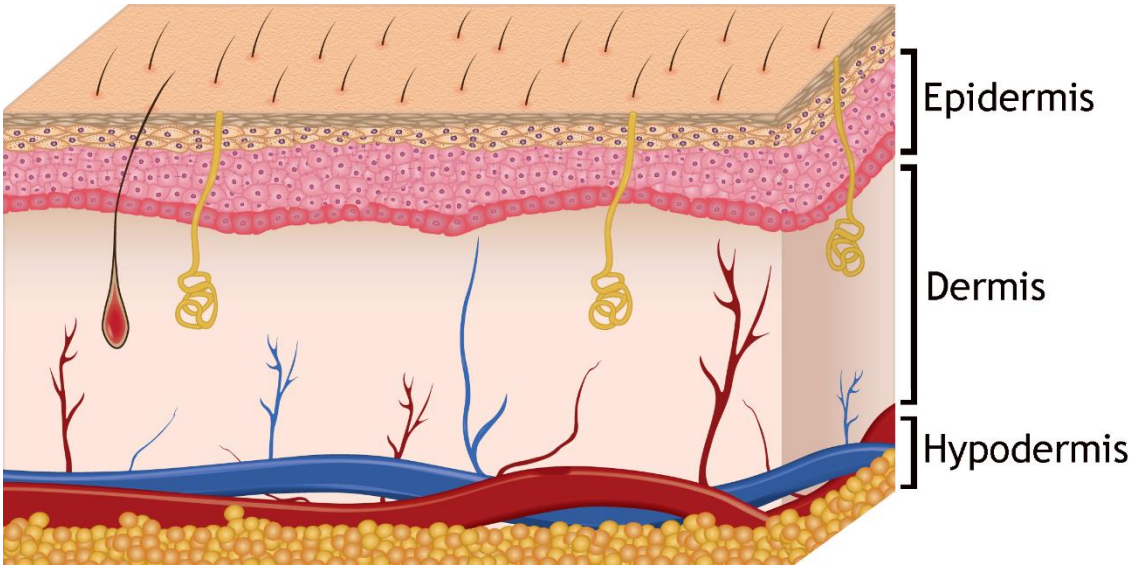

Figure 1. Schematic representation of the skin' structure.

1.2. Wounds

A wound can be defined as a disruption of the structural and functional integrity of the skin due to physical, chemical, mechanical and/or thermal damage [14]. Further, wounds may also be associated with obesity and diabetes [1, 15]. Additionally, wounds can be classified into superficial partial-thickness, deep partial-thickness or full-thickness, according to the depth and the layers of the skin that are affected [16]. A representation of the different types of wounds are depicted in the Figure 2.

Superficial wounds only affect the surface of the epidermis layer, and they are capable of healing without scarring, in 10 days, through re-epithelization [16, 17].

Deep partial-thickness wounds comprise the damage of the epidermis as well as the dermis, which may include blood vessels, sweat glands and hair follicles. In this type of wounds, the scarring is more pronounced and the heal occurs in 10-21 days, through a re-epithelization process [16-18].

On the other hand, the full-thickness wounds occur as a consequence of the damage of the epidermis, dermis, skin appendages, and hypodermis. The healing process of these type of wounds involves the formation of granulation tissue, re-epithelization and it usually requires more than 21 days [16-18].

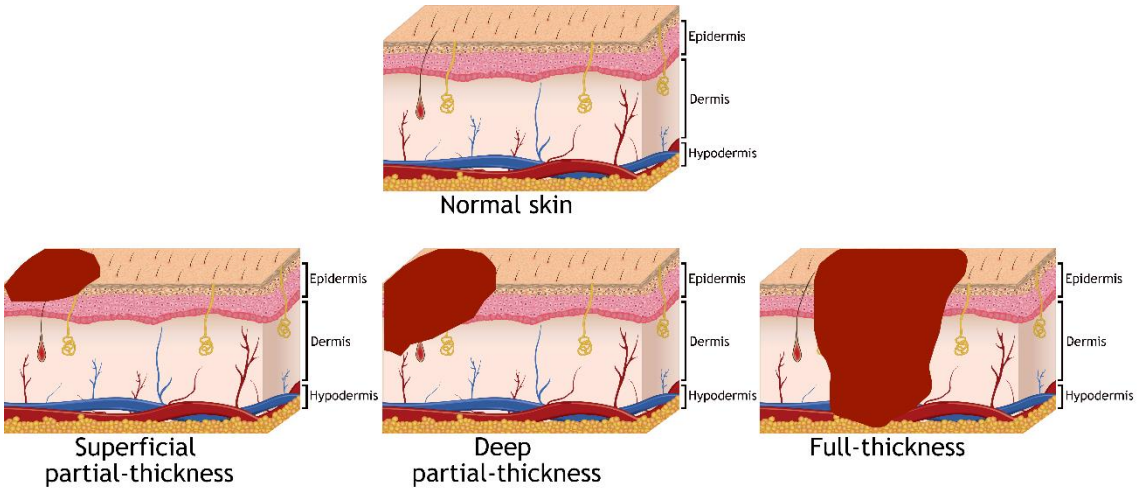

Figure 2. Illustration of the different types of skin injuries: superficial partial-thickness (when only the surface of the epidermis layer is damaged), deep partial-thickness (epidermis and dermis are both damaged) or full-thickness wounds (epidermis, dermis, skin appendages and hypodermis structure are disrupted).

1.3. Wound Healing

Wound healing is a complex and dynamic process that can last several weeks, depending on the size, depth and location of the wound and patient's general health condition [19, 20]. The wound healing process involves five different phases, namely hemostasis, inflammation, migration, proliferation and remodelling (represented on Figure 3) [21].

1.3.1. Hemostasis

When skin suffers an injury, the hemostasis is initated with the production of a provisional matrix at wound site to stop the bleeding. As a consequence, the coagulation cascades are activated and the platelet aggregration occurs [22]. Then, a blood clot composed of fibrin, fibronectin, vitronectin, and thrombospondin is formed [1, 23]. Furthermore, thrombin, collagen and platelets stimulate the production of transforming growth factor-β (TGF-β), platelet-derived growth factor (PDGF), platelet activation factor, serotonin and fibronectin. Then, TGF-β and PDGF contribute to attract macrophages, neutrophils, fibroblasts, endothelial cells, and smooth muscle cells to the wound site, that play pivotal roles during the wound healing process [22, 24].

1.3.2. Inflammation

Subsequently, the inflammatory phase begins and it is characterized by the migration of neutrophils, macrophages and lymphocytes to the lesion site, in order to clean the wound from the necrotic tissues and to prevent the infection [19]. Initially, the secretion of proinflammatory cytokines (interleukin-1β (IL-1β), tumor necrosis factor-α (TNF-α) and interferon-γ (IFN-γ)) stimulate the recruitment of neutrophils to the wound, that are involved in the elimination of microorganisms present at the wound site through phagocytosis [25, 26]. Furthermore, these cells are also responsible for degrading matrix proteins and attract inflammatory cells, by expressing proinflammatory cytokines, reactive oxygen species (ROS), cationic peptides, and proteases at the injury site [22, 26]. Then, monocytes also migrate into the wound and differentiate into macrophages, attaining their higher concentration at 48-72h after injury [23, 25]. The macrophages are also phagocytic cells that secrete TGF-α, TGF-β, basic fibroblast growth factor (bFGF), PDGF, and vascular endothelial growth factor (VEGF). These cytokines and GF are also involved in the regulation of the inflammatory process, stimulation of angiogenesis and attraction of keratinocytes, fibroblasts and endothelial cells [1, 23, 25]. After 72h, the lymphocytes migrate to the wound site, helping in the production of ECM [25].

1.3.3. Migration Phase

The migration phase begins at 2-10 days after skin injury occurs and it is characterized by the re-epithelization, neovascularization and formation of granulation tissue. The cells migrate from the margins to the injured area and promote the production of matrix as well as the formation of granulation tissue [21].

1.3.4. Proliferation Phase

In the proliferation phase, fibroblasts present at the wound site produce collagen, elastin, fibrin, and fibronectin [22, 27]. These ECM proteins allow the formation of a temporary matrix that is essential for angiogenesis, and for the remodelling phase to occur [26, 27]. Further, fibroblasts also secrete bFGF, that in combination with VEGF (secreted by platelets and neutrophils), stimulate the endothelial cells proliferation and migration. Such cells are responsible for the formation of new blood vessels, which are crucial to promote the nutrient and oxygen exchange [1, 27].

1.3.5. Remodelling

Finally, the remodelling phase occurs after 2-3 weeks, and may last to 2 years. This phase is characterized by the reorganization, degradation and synthesis of new ECM [26, 27]. At this stage, TGF-β stimulates the expression of smooth muscle actin by fibroblasts and they differentiate into myofibroblasts, that are responsible for the wound contraction [23, 27]. Moreover, the type III collagen is replaced by type I collagen in order to increase the tensile strength of the skin [1]. Also at this stage, the proportion of proteoglycans and water decreases, while the amount of elastin increases leading to an increase of skin's elasticity. In the final stage of wound healing process, the apoptosis of vascular and myofibroblasts cells occurs and the cell-rich granulation tissue is converted into a hypocellular scar [23].

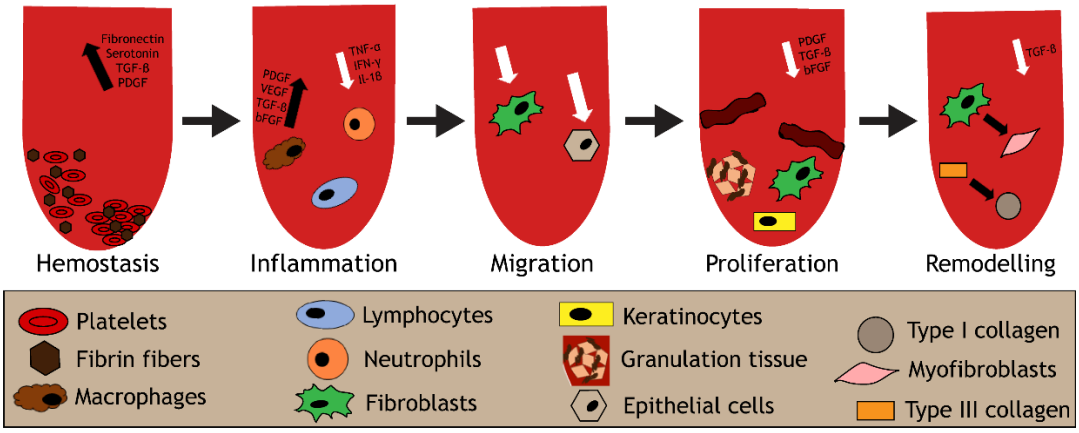

Figure 3. Illustration of the main phases of the wound healing process. The hemostasis is characterized by the stimulation of the platelet activation, adhesion and aggregation as well as the production of TGF-β, PDGF, serotonin and fibronectin; The inflammatory phase is characterized by the migration of inflammatory cells (neutrophils, macrophages and lymphocytes); In the migration phase, the epithelial cells and fibroblasts migrate to the wound site; In the proliferative phase, the activity of the fibroblasts and keratinocytes contribute for the formation of the granulation tissue and the neovascularization; The remodelling phase is characterized by the reorganization, degradation and synthesis of new ECM, which include the differentiation of the fibroblasts into myofibroblasts and the replacement of type III collagen by type I collagen.

1.4. Tissue Engineering and skin substitutes

When the area and depth of the skin lesion are extensive, the human body is unable to repair the skin by itself, demanding the use of dressing materials to cover and protect the wound, while the structure and functions of this organ are re-established. Skin grafts, that include autografts, allografts and xenografts have been the most used for this purpose [19, 28]. Autografts remain as the gold standard treatment used for skin replacement and repair, since it is able to: i) cover the injured area; ii) remains during a long period at wound site; and iii) do not present risk of rejection [19, 29]. Although, this type of grafts display a limited availability and its obtention induce pain in the patient [19, 30]. On the other hand, allografts, obtained from cadavers or living donors, have a higher availability than autografts while retaining native features of skin, like structure, mechanical properties and it may be revascularized [29, 31]. However, these grafts have some bottlenecks such as high cost and a high risk of transmission of infectious diseases [28, 31]. Xenografts are obtained through the harvesting of a skin portion from another species. This type of grafts have several benefits such as decreased water loss, sustain a moisture environment at the wound site and the low price. However, they have associated immune rejection issues [28, 31, 32].

1.4.1. Wound dressings

Due to the limitations displayed by the currently available grafts, researchers from the tissue engineering area are investigating different alternatives to develop wound dressings that are capable of mimicking the features of the native skin, while improving the wound healing process. In this way, the wound dressing should: i) provide a moist environment at the injured site; ii) stimulate cell proliferation and migration; iii) improve the angiogenesis; iv) protect the wound against microorganisms invasion, which are responsible for triggering infections; v) allow exchange gases and fluids; and vi) be biocompatible, biodegradable, non-toxic and cost-effective [3, 20, 27, 33]. Considering these properties, wound dressings are usually grouped into three different groups: passive, interactive and bioactive (presented in Table 1) [33].

1.4.1.1. Passive wound dressings

Passive dressings are dry dressings, that are usually used to clean and protect wounds with a reduced amount of exudate. However, they do not provide a moist environment and require frequent changes to protect the wound against external agents

(microorganisms, physical/chemical damage) as well as skin maceration. Furthermore, the recurrent changes of these dressings may lead to the formation of new lesions, tissue exacerbation, increased risk of infection and pain to the patient. Passive dressings include gauzes, lint, plasters and cotton [33, 34]. The gauzes are the most commonly used traditional dressings and they are made of woven and nonwoven fibers of cotton, rayon polyester or a combination of both. These dressings can be used to absorb blood and exudate and clean the wound site during the initial stages of the wound healing process. Moreover, the gauzes have a low cost associated, although they may adhere to the wound, due to the excessive wound drainage, leading to an increased pain to patients during its removal. Due to such properties, gauzes are usually used to clean and dry wounds or as secondary dressings in order to absorb exudate and protect the wound [21, 34].

1.4.1.2. Interactive wound dressings

To surpass the drawbacks of the passive dressings namely, their incapacity to sustain a moist environment at the wound site and their frequent replacement during the period of the treatment, interactive dressings have been developed. This type of dressings are produced to confer and maintain a moist wound environment, improving the healing process, as well as provide a barrier against microbial invasion and UV radiation. These wound dressings are semi-occlusive or occlusive and are widely used for the treatment of moderate to severe acute and chronic wounds. Films, hydrogels and hydrocolloids are some examples of interactive wound dressings [33, 34]. Films are semi-permeable dressings, which enable the transmission of gases, and due to its flexibility can acquire the shape of the wound. Moreover, transparent materials, like polyurethane (PU) have been used for the production of films. This type of dressings allow the monitoring of the healing process, without requiring its removal. On the other hand, hydrogels have a high water content, which enables them to maintain a moist environment at the wound site. Further, the elasticity exhibited by hydrogels allow their easy application and removal, without inducing any damage to the patient. However, they present weak mechanical properties and its high exudate absorption capacity can compromise the moist content at the injury site and may lead to wound maceration [33]. In the same way, the hydrocolloids are skin substitutes that are permeable to water vapor and display a high capacity to absorb the wound exudate. Hydrocolloids gellify when they are in contact with fluids available in the wound, namely wound exudate. However, in some situations the excessive exudate absorption may lead to the maceration of the surrounding tissues [33, 34].

1.4.1.3. Bioactive wound dressings

Nowadays, researchers have been enrolled in the development of bioactive dressings containing biomolecules or antimicrobial agents that have crucial roles for improving the biological activity as well as the cellular response. Some of these bioactive dressings are already available for clinical use and they are classified according to the skin layer that they are able to regenerate, namely epidermal, dermal or dermal-epidermal substitutes [34].

1.4.2. Skin substitutes

1.4.2.1. Epidermal substitutes

Epidermal substitutes were the first ones to be produced and they are aimed to mimic the epidermal layer of the skin and may contain keratinocytes cells [35]. Some of the epidermal skin substitutes contain autologous or allogenic keratinocytes [36]. Epicel® is an example of an epidermis substitute composed of sheets of autologous keratinocytes seeded in a gauze support that is removed 1 week after the transplantation to the wound site. Other commercial epidermal skin substitutes are MySkin®, a synthetic silicone support layer seeded with autologous keratinocytes and Epidex® that presents autologous keratinocytes, from outer root sheet of patient's hair follicles, in silicone membranes [35].

1.4.2.2. Dermal substitutes

Dermal substitutes were developed in order to fill the lack of dermal tissue in deep wounds and to improve the quality of scars after their treatment with split thickness autografts or cultured epithelial grafts. Dermal substitutes mimic the dermis layer of the skin and could be cellular or acellular. They are conceived to support cell growth, migration, revascularization, and neodermis formation [36].
Different dermal substitutes are available in the market, namely: Biobrane® which is a synthetic bilayer acellular skin substitute, composed of a three-dimensional (3D) nylon filament incorporating type I porcine collagen, and a semipermeable silicone film, that is able to control the skin fluid loss; Integra®, an acellular dermal substitute that is composed of crosslinked bovine tendon collagen, glycosaminoglycan and a semi-permeable polysiloxane layer; Dermagraft® which is composed of a poly(lactide-co-glycolide) (PLGA) mesh scaffold with neonatal dermal fibroblasts; TransCyte® that consists of a nylon mesh covered with porcine dermal collagen seeded with neonatal fibroblasts [35, 36].

1.4.2.3. Dermal-epidermal substitutes

Dermal-epidermal substitutes are aimed to mimic both layers of the native skin. These bilayered skin analogs possess in their constitution autologous or allogenic keratinocytes and fibroblasts, which are responsible for GF and cytokines secretion and ECM deposition [36]. Apligraf® is an example of a dermal-epidermal substitute, which is composed of a bottom dermal layer of bovine type I collagen seeded with human fibroblasts, and a top epidermal layer formed by a culture of human keratinocytes. In addition, there are other examples of dermo-epidermal skin substitutes available in the market like the PermaDerm™, that is composed of a collagen base cultured with fibroblasts and keratinocytes, whereas the OrCel® is a bilayer type I collagen sponge seeded with allogenic keratinocytes and fibroblasts [35, 36].

Despite of the advantages presented by the skin substitutes, they still present some limitations that need to be overcome, such as: i) avoid the use animal-derived materials; ii) improve the adhesion of cultured keratinocytes to the wound bed; iii) improve the rate of neovascularization; iv) enhance the mechanical properties; v) enhance the cost-effectiveness [35, 36].

1.4.3. Wound dressings under development

In order to overcome the shortcomings of the currently available dressings, researchers are using biodegradable and natural polymers (collagen, HA, chitosan (CS), alginate, elastin) to produce new types of dressings [34]. The use of the natural compounds-derived polymers intends to activate/direct a cellular response in order to improve the healing process as well as preventing possible antibacterial infections [33]. In this way, antimicrobial peptides, stem cells, GF, vitamins and other agents have been incorporated into the wound dressings, due to its active role during the healing process [37]. Lu *et al.* produced a chitosan-gelatin sponge crosslinked with tannin acid (CSGT), using a freeze-drying technique, and posteriorly, incorporated platelet-rich plasma (PRP) into the 3D matrix [38]. These authors started by evaluating the bactericidal activity of the chitosan sponge (ChS), gelatin sponge (GS) and CSGT, using *Staphylococcus aureus* (*S. aureus)* and *Escherichia coli* (*E. coli)*, as bacteria models. The results obtained in their study show that ChS and CSGT were able to inhibit the bacterial growth of both species. However, no inhibitory effect was noticed for bacteria in contact with GS samples, once the antibacterial property was conferred by CS. Further, CSGT presented better results compared to ChS, due to the presence of tannic acid. In addition, the *in vivo* assays showed that the wounds treated with CS presented a slow recovery, since the epidermis

layer did not properly regenerate. The sponge adhered to the wound and its removal induce damage at the wound site. On the other hand, the CSGT and CSGT loaded with PRP were easily removed and improved the healing process, since epidermis and dermis were almost fully repaired, after 15 days [38]. In turn, Zhang and their collaborators fabricated hydrogels (composed of arabic gum, pectin and Ca^{2+}) loaded with bFGF aiming to stimulate wound healing process [39]. The analysis of bFGF release profile from the bioinspired hydrogels, showed an initial burst release followed by a sustained release along 12h. In this way, these two-stage bFGF release profile enables the control of the early and of the later stages of the wound healing process. Furthermore, the *in vivo* assays demonstrated that the bioinspired hydrogels with bFGF enhanced the wound contraction (60%), in comparison to the control group and bioinspired hydrogels without bFGF (27% and 42%, respectively), after 3 days of treatment. In addition, the wounds treated with bioinspired hydrogels containing bFGF showed a complete formation of the new epithelium, a highest fibroblast density, production of ECM proteins and collagen deposition [39].

Tang *et al*. produced a PLGA nanofibrous mesh and then seeded human adipose-derived stem cells on its surface [40]. After that, the authors evaluated the viability of human adipose-derived stem cells and L929 fibroblasts on PLGA nanofibrous meshes, and they confirmed the biocompatibility of the produced mesh. Further, the *in vivo* assays revealed that the PLGA nanofibrous mesh seeded with cells was able to improve the wound healing process, since the wound was completely closed after 14 days [40].

Among of the wound dressings produced so far, those composed of nanofibers are receiving an increasing attention, due to their fibers' small diameter, high surface area and high porosity, which allow an efficient gas exchange, nutrient supply and an easy incorporation of bioactive molecules as well as impaired penetration of microorganisms [33, 37]. The nanofibers can be produced using different techniques, such as self-assembly, phase separation and electrospinning. Among these techniques, electrospinning has been the most used due to its versatility, simplicity, low cost and possibility of using different polymers, that enable the production of multifunctional dressings that are capable of mimicking the ECM [41].

Table 1. Classification of the available wound dressing.

Category	Properties	Wound type	Products	Advantages	Disadvantages	Commercials	References
Passives	- dry bandages that cover the wound during the healing process.	- superficial and clean wounds with low exudate.	- gauzes, lint, plasters, cottons.	- protection against trauma or external agents.	- requires frequent changes; - adhere easily to the wound; - its removal from wound site can induce trauma ; - do not control moisture levels.	Jelonet®, Paratulle, Tullegras, Unitulle, Urgotul™, Atrauman®, Mepilex®, Mepitel®, Tegapore™, Tricotex®, etc.	[33, 37, 42]
Interactives	- provide and maintain a moist wound environment, that improves the healing process.	- acute and chronic wounds, moderate to severe, with small to large exudates.	- films, hydrogels, hydrocolloids.	- allow the transmission of gases; - its flexibility allow them to adapt to the shape of the wound; - control moisture levels; - protection against trauma or some agents.	- weak mechanical resistance; - provide suitable environment for bacterial growth; - can induce maceration.	Bioclusive®, Cutifilm, Mefilm®, Tegasorb™, Aquacel®, Versiva®, Aquaform®, GranuGel®, Purilon®, Sterigel®, Tegaderm™, Comfeel®, Granuflex®, Opsite, etc.	[21, 33, 37, 42]
Bioactives	- activate/direct a cellular response, and prevent possible bacterial infections.	- severe acute and chronic wounds, both clean or infected.	- skin substitutes loaded with biomolecules or antimicrobial agents.	- high elasticity and flexible; - protection against contamination; - regulate wound healing through active substances; - control the moisture levels.	- high costs of the fabrication; - demand the optimization of the drug release.	Acticoat®, Iodoflex®, Integra®, Aloderm®, Dermagraft®, Promogran®, Regranex®, TransCyte®, Biobrane®, Epicel®, Apligraf®, etc.	[33, 37, 43-45]

1.5. Electrospun Membranes

Electrospinning is a technique that allows the production of polymeric nanofibers, leading to the formation of membranes displaying an interconnected 3D network that mimics the ECM [41, 46, 47]. Up to now, this technique has been widely used by researchers due to its simplicity, low cost, versatility, and suitability for the production of membranes with high surface area-to-volume ratio and porosity [41, 46]. The high surface-area-to-volume ratio exhibited by these nanofibers contributes for a higher adsorption capacity, about 8 to 92 times higher than other traditional dressings, as well as promotion of cell attachment. Further, the higher porosity exhibited by these membranes also allows gas exchange, nutrient supply and fluid loss control [33, 41, 47]. These properties ensure a moist environment at the wound site. In this way, the nanofibrous membranes are capable to prevent patient's dehydration, stimulate cell migration, adhesion, proliferation and differentiation, improving angiogenesis [41, 48]. Furthermore, these membranes can also incorporate bioactive molecules, such as therapeutic or antimicrobial agents, that enhance their biological activity, through different production techniques: pre-electrospinning (*e.g.* blend, co-axial and emulsion) and post-electrospinning (*e.g.* physical adsorption, layer-by-layer assembly and chemical immobilization) [33, 41].

1.5.1. Electrospinning set-up used to produce the electrospun membranes

The electrospinning apparatus is usually composed of four components: a syringe pump, a capillary needle, a high voltage power supply and a metal collector (see Figure 4) [41]. The process starts with the creation of an electric field between the needle and the collector. When it reaches a critical value, the reciprocal repulsion of loads occurs, which produce a force that opposes to the surface tension. This oppositely force leads to the ejection of the solution in the direction of the field. Thus, the polymer droplets deform and form the Taylor cone and, consequently, the solvent evaporates and the nanofibers are deposited into the collector [33, 47, 49].

Electrospinning process is controlled by several parameters, such as: i) solution parameters (*i.e.,* polymer concentration, viscosity, solvent volatility, surface tension and conductivity); ii) environmental parameters (*e.g.* temperature and humidity); and iii) operating parameters (*e.g.* applied voltage, flow and distance to collector). It is worth to notice that these parameters require optimization, since they play a critical role in the properties exhibited by the membranes, including on fibers' diameter and arrangement, mechanical strength and porosity [33, 41]. Furthermore, the type of collector (stationary

or rotating) also influences the arrangement of the fibers. For example, membranes produced using a stationary collector will present a high porosity, random orientation and a morphological structure that mimics the collagen fibers structure found in the normal skin ECM, while a rotating collector allows a specific orientation of the fibers, *i.e.*, the nanofibers are produced with a specific orientation like the ECM found on muscle and nervous tissue [41].

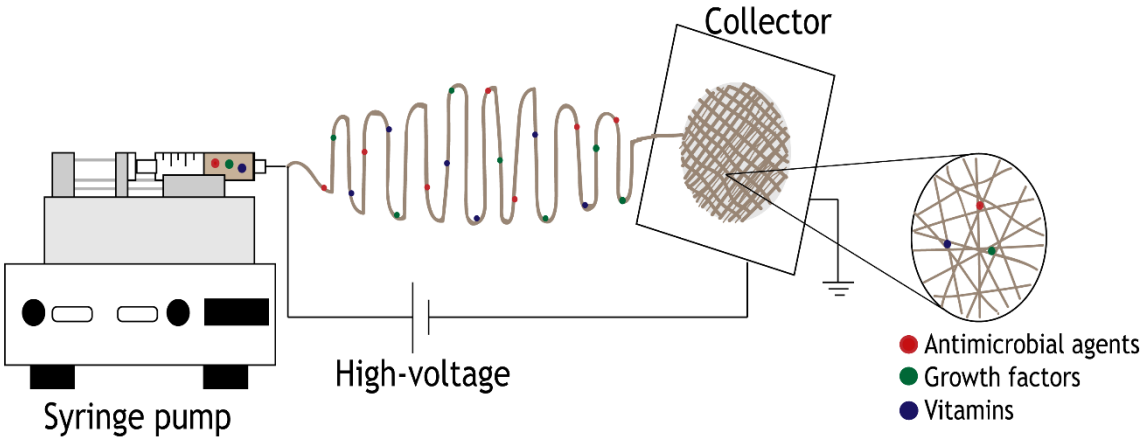

Figure 4. Illustration of a conventional electrospinning apparatus used for the production of electrospun membranes, with/without incorporation of bioactive molecules (*e.g.* antimicrobial agents, GF and /or vitamins).

1.5.2. Asymmetric electrospun membranes

The electrospinning technique also allows the production of several layers, through the deposition of one layer above another. This possibility combined with the use of different polymers to produce the layers allows a better reproduction of the native skin' structure. In this way, tissue engineering researchers have been producing different asymmetric membranes through electrospinning in order to mimic both layers of the skin. The epidermis side is usually composed of a dense layer that provides a protective barrier from external hazard agents. On the other side, the dermis is conceived to promote a moist environment that promotes cell migration, adhesion, and proliferation [50, 51]. Figueira *et al.* produced a bilayered membrane composed of a top layer of HA_poly(caprolactone) (PCL) and a bottom layer of CS_zein (ZN)_salicylic acid (SA) [52]. The porosity studies revealed that the HA_PCL layer presented a porosity value below 90%, which is crucial to avoid the bacterial contamination. On the other hand, the CS_ZN_SA layer had a porosity value of 162.35 ± 34.68%, that is considered suitable for cell migration and gases/nutrients/fluids exchange. Finally, the bilayer membrane presented an inhibitory effect of ≈99% against *S. aureus*, avoiding biofilm formation at the membrane's surface [52]. In turn, Miguel *et al.* produced an electrospun asymmetric membrane, where silk fibroin (SF) and PCL were mixed to produce the top layer, while a

SF_HA_thymol (THY) blend was used to produce the dermis bottom layer [53]. The mechanical properties (Young's modulus, tensile strength, and elongation at break) exhibited by the produced membrane were similar to those of native skin, demonstrating that this membrane is capable of providing mechanical support during wound healing process. Moreover, the SF_PCL top layer presented a porosity of 64.28 ± 2.59%, which is suitable for avoiding the microorganism invasion, while the SF_HA_THY bottom membrane presented 85.24 ± 2.47% of porosity, that enhances cell migration, adhesion, and proliferation. On the other hand, the bottom layer exhibited a higher swelling ratio than the top layer, due to the incorporation of HA, which is fundamental for the absorption of the wound exudate as well as to prevent tissue maceration. In addition, the SF_PCL exhibited an hydrophobic character, with a water contact angle (WCA) of 103.10 ± 6.57º, while the SF_HA and SF_HA_THY membranes presented WCA values of 26.51 ± 4.87º and 38.77 ± 5.32º, respectively. This hydrophilic character shown by these membranes is a requirement for supporting cell attachment and proliferation. The incorporation of the THY into the bottom layer of the asymmetric membrane improved its antioxidant and antibacterial properties [53].

In another study, Sheng-Han *et al.* developed a dual-layer electrospun CS/poly(D,L-lactic acid) (PDLLA) membrane [54]. The top layer was composed of aligned CS nanofibers, whereas the bottom layer was comprised of random PDLLA microfibers. The dual-layer electrospun membrane presented a surface pore size of about 12.18 ± 1.7 μm, that improves cell infiltration and growth. Moreover, *in vivo* assays demonstrated that PDLLA, CS and CS/PDLLA dual-layer membrane allowed a faster restoration of skin structure and functions than gauze or a PDLLA film. Such result can be explained by cellular infiltration up to 32.5 μm depth, a feature that increases the rate of epidermis and dermis layers restoration [54].

1.5.3. Polymers used to produce the electrospun membranes

A strategy widely used by researchers to produce electrospun membranes, is based on the combination of natural and synthetic polymers aiming to better mimic the functions and structure of the native skin. Natural polymers (*e.g.* collagen, CS, alginate, HA, cellulose acetate (CA)) have been selected due to their biocompatibility, biodegradability and similarity to cell-recognized macromolecules. On the other hand, synthetic polymers (*e.g.* PCL, poly(vinyl alcohol) (PVA), PU, polylactic acid (PLA)) are easily electrospun and present excellent mechanical properties, like strength, flexibility and rigidity [47, 48].

1.5.3.1. Poly(caprolactone)

PCL is a semi-crystalline aliphatic polyester (its chemical structure is depicted in Figure 5), that exhibits features like biocompatibility, chemical and thermal stability, and good mechanical properties which are essential for tissue engineering applications. Furthermore, PCL is biodegradable and the products resulting from its degradation are non-toxic [55-57]. In addition, this polymer is already approved by the Food and Drug Administration for biomedical applications.

In the wound healing area, PCL has been widely used in the production of dressings through electrospinning. This synthetic polymer allows the production of ultrafine nanofibers, that provide a high porosity and surface area. However, the high hydrophobic character of this polymer hinders cell adhesion and proliferation [48, 57]. In this way, researchers of tissue engineering area have been searching for solutions to overcome this disadvantage. Mahboobeh *et al.* produced PCL/gelatin (Gel) nanofibers with different concentrations of lawsone (Law) (0.5%, 1%, 1.5%), using coaxial electrospinning. The membrane's hydrophilicity was enhanced by performing an O_2 plasma treatment of membrane's surface [58]. The biodegradation profile of the membranes was characterized in phosphate-buffered saline (PBS), over 14 days, and the results revealed a degradation of ≈17%, ≈27%, ≈39% and ≈14% for PCL/Gel/Law 0.5%, PCL/Gel/Law 1%, PCL/Gel/Law 1.5% and PCL/Gel membranes, respectively. A tensile strength of 2.14 ± 0.3 MPa, 1.7 ± 0.9 MPa, 1.217 ± 1.4 MPa and 0.84 ± 0.8 MPa was determined for the PCL/Gel and PCL/Gel/Law (0.5, 1, 1.5%) membranes, respectively. Finally, the wound healing performance of the membranes was also evaluated in rats and after 14 days, the wound closure rate was 66.4 ± 3.6%, 71.4 ± 2%, 96.3 ± 4% and 100 % for the negative control (without any treatment be administered), PCL/Gel, PCL/Gel/Law 1% and 1.5% nanofibers, respectively [58].

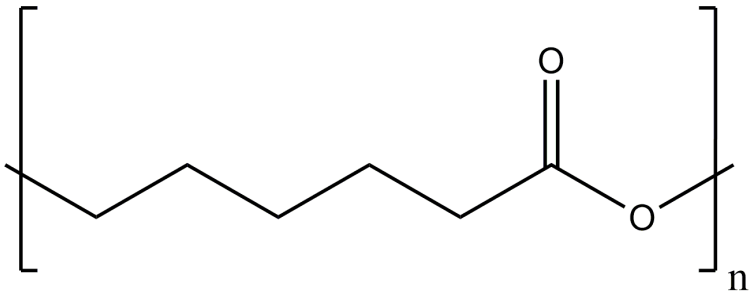

Figure 5. Representation of molecular structure of poly(caprolactone).

1.5.3.2. Poly(vinyl alcohol)

PVA is another synthetic polymer (Figure 6) that has been widely used in the biomedical field for different purposes due to its properties, such as biocompatibility, biodegradability, good mechanical performance, low cost and availability [20]. Furthermore, its hydrophilic character confers it a swelling behaviour that allows PVA to absorb wound exudate as well as maintain a moist environment. However, the rapid disintegration of PVA into aqueous solutions is a limitation, which has been circumvented by the PVA chemical crosslinking [33, 59].

Mohammad and their collaborators produced electrospun PVA/Schizophyllan (SPG) nanofibers and then, crosslinked them with glutaraldehyde aiming to enhance membranes aqueous stability [60]. The authors characterized the swelling capacity of the produced membranes and the results obtained revealed values of 105.1 ± 4%, 289 ± 14%, 318.4 ± 6% and 338 ± 12% for PVA, SPG/PVA-20, SPG/PVA-30 and SPG/PVA-40 membranes, respectively. Further, the produced nanofibers exhibited tensile strength values (3.322 ± 0.9 MPa, 6.513 ± 0.53 MPa, 5.632 ± 0.7 MPa and 3.039 ± 0.42 MPa for PVA, SPG/PVA-20, SPG/PVA-30 and SPG/PVA-40 membranes, respectively) similar to those presented by the native skin (5.00–30.00 MPa). In addition, the authors also verified that the produced membranes did not induce any cytotoxic effect on L929 fibroblasts cells after 72 hours of incubation [60]. Ganesh *et al.* produced CS/PVA/silver nanoparticles (AgNPs) electrospun nanofibers loaded with sulphanilamide that were aimed to enhance wound healing process [61]. The *in vivo* results demonstrated that the control group showed very slow healing even after 20 days (55.26 ± 3.5% of wound contraction). On the other hand, the wounds treated during 7 days with CS/PVA nanofibers exhibited a wound contraction percentage of 90.76 ± 4.3% , while with the CS/PVA/AgNPs nanofibers loaded with sulphanilamide presented a maximum rate of wound healing (≈ 100% of the wound contraction was obtained) [61].

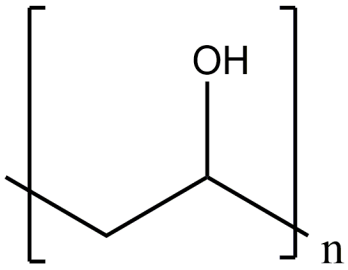

Figure 6. Representation of molecular structure of poly(vinyl alcohol).

1.5.3.3. Cellulose acetate

Cellulose is one of the most common biopolymers found on earth and researchers from different areas have been investigating its derivatives (cellulose ethers/esters, micro/nano-sized cellulose products, etc), to surpass its limited solubility in organic solvent [62].

Among the different cellulose derivatives, CA (Figure 7) is the most used in the biomedical applications, due to their intrinsic properties such as thermal stability, chemical resistance, biocompatibility, biodegradability, mechanical resistance and low cost [63].

Based on its intrinsic properties, CA has been widely investigated by researchers for the production of nanofibrous membranes, aiming to improve the wound healing process. Vatankhah and their collaborators fabricated CA/Gel membranes through electrospinning using different ratios of CA/Gel (CA/Gel75:25, CA/Gel50:50 and CA/Gel25:75) to obtain a skin substitute for the treatment of superficial and deep wounds [64]. These authors noticed that the membranes possessed an average fiber diameter (198–260 nm) and a pore size (0.77–1.16 mm) compatible with cell adhesion, exchange of nutrients and metabolites, as well as absorption of exudate. In addition, the membranes demonstrated a biocompatible profile that promotes cell adhesion and proliferation of human dermal fibroblasts at their surface [64]. In a similar way, Samadian *et al.* produced CA/Gel nanofibrous membranes through electrospinning, incorporating nanohydroxyapatite at different concentrations to be used as wound dressings [65]. The *in vivo* assays performed by these authors revealed that the nanofibrous membranes induced the re-epithelization and improved the wound closure in comparison to the control group (sterile gauze). Further, the CA/Gel membrane loaded with nanohydroxyapatite displayed the best results, *i.e.,* animals revealed a higher collagen synthesis, re-epithelization, neovascularization and also the greatest cosmetic appearance. In this way, the CA/Gel/ nanohydroxyapatite electrospun nanofibrous showed suitable properties for improving the healing process [65].

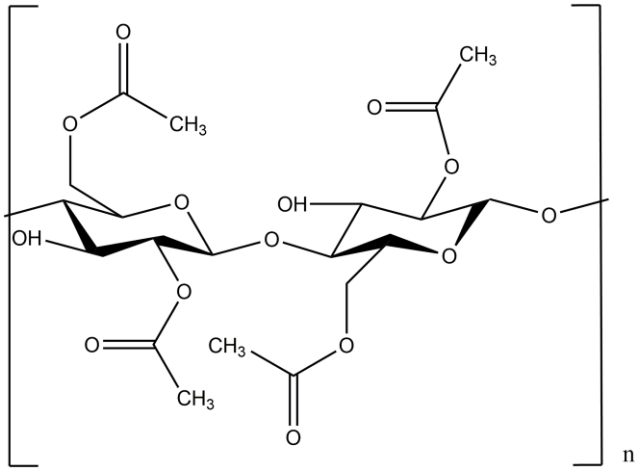

Figure 7. Representation of molecular structure of cellulose acetate.

1.5.3.4. Hyaluronic acid

HA, one of the main components of skin ECM, is a non-sulfated glycosaminoglycan composed of repeated disaccharide units of β-D-glucuronic acid and N-acetyl-D-glucosamine (the chemical structure of HA is presented in Figure 8) [66]. The presence of the large number of carboxyl and hydroxyl groups in the HA structure confer it a highly hydrophilic character. This feature allows HA to absorb exudate as well as enhance cell adhesion [67]. In addition, HA is also involved in the hemostasis phase, it prompts the deposition of fibrinogen and the formation of the initial clot. Further, it is also enrolled in the regulation of the inflammatory phase and encourage the re-epithelization process, thus contributing for the proliferation of fibroblasts and keratinocytes, as well as to the activation of macrophages and lymphocytes, through interleukins, proinflammatory cytokines or binding to a receptor [68, 69]. Moreover, the performance of HA in the wound healing process is dependent on HA molecular weights, *i.e.,* high molecular weight HA exhibit anti-inflammatory activity, while HA with low molecular weight is pro-angiogenic, *i.e.* stimulates the production of proinflammatory cytokines and GF that are involved in skin ECM remodelling [66]. So, due to HA intrinsic properties (such as biocompatibility, biodegradability and hydrophilic character) and its performance in the wound healing process, it has been widely used for the production of different wound dressings [67].

Chanda *et al.* produced a CS/PCL-HA bilayered membrane, that was crosslinking with glutaraldehyde vapor for 18h, in order to obtain a membrane with an improved mechanical stability and wound bed hydration [70]. The CS/PCL-HA bilayered membrane exhibited fibers with average diameter value of 362.2 ± 236 nm, which is similar to that found in collagen fibers of ECM (50 to 500 nm), and enhanced the cell adhesion, proliferation and differentiation. The obtained swelling capacity was ≈135%

for CS/PCL-HA bilayered membrane, thus demonstrating its high capacity to absorb the excess of wound exudate. Furthermore, these authors also verified that the CS/PCL-HA membranes possess the WCA (82.4 ± 6.4°), water vapor transmission rate (WVTR) (≈2500 ml/m²/day), porosity values (>90%) and biocompatible profile suitable to be used as wound dressings [70]. In another study, Shin *et al.* produced co-axial nanofibers of HA and PLGA loaded with epigallocatechin-3-O-gallate (HA/PLGA-E), aiming to use them for the treatment of full thickness wounds [71]. The data obtained in their study revealed that the animals treated with HA/PLGA-E membranes presented a lower wound size after 14 days of treatment, in comparison with the other groups. Such results suggest that a synergistic effect occurs between HA and epigallocatechin-3-O-gallate, which can improve the healing process by scavenging ROS, mitigating inflammation, enhancing the re-epithelization, promoting angiogenesis and the ECM reorganization [71].

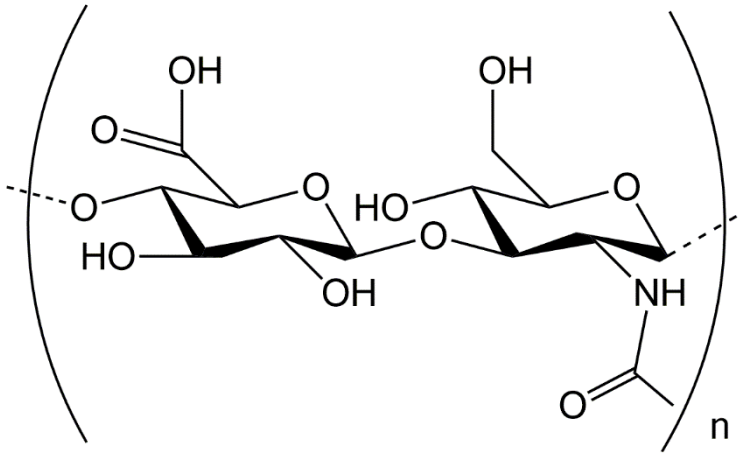

Figure 8. Representation of the molecular structure of hyaluronic acid.

1.5.4. Electrospun membranes as drug delivery systems

As described above in the text, one of the characteristics/advantages of nanofibrous membranes is the possibility to incorporate bioactive molecules within their mesh. When these membranes are used as drug delivery systems, their biodegradation leads to the release of the incorporated molecules. Different methods including pre-electrospinning techniques (*e.g.* blend, co-axial and emulsion) and post-electrospinning techniques (*e.g.* physical adsorption, layer-by-layer assembly and chemical immobilization) have been used for membranes production. Furthermore, the surface of electrospun membranes can be chemically and physically modified with bioactive molecules and ligands (recognized by cells) for improving their effectiveness during the healing process. Among these bioactive molecules, antimicrobial agents, stem cells, GFs and vitamins have been the most incorporated [41].

1.5.4.1. Electrospun membranes with antibacterial activity

When the skin integrity is disrupted, the occurrence of infections lead to the deterioration of the granulation tissue, GF and ECM components and, consequently, to the impairment of the wound healing process. Skin and soft tissue infections have a high incidence and morbidity associated. These infections can be caused by different bacteria, *i.e.*, in initial stages infections occur as a consequence of gram-positive bacteria, such as *S. aureus,* while in later stages they are originated by gram-negative bacteria, such as *E. coli* and *Pseudomonas aeruginosa (P. aeruginosa)*. In this way, dressings incorporating different antimicrobial agents have been developed, such as antibiotics, nanoparticles (*e.g*. silver, chitosan, iron oxide, nitric oxide) and natural products (*e.g*. honey, essential oils and CS), to prevent bacterial infection [72, 73].

1.5.4.1.1. Silver nanoparticles

The biological, high conductivity and thermal properties exhibited by AgNPs propelled their application in different areas [74]. The bactericidal activity displayed by these nanoparticles constitutes an alternative to conventional antibiotics without triggering microbial resistance [73]. Different mechanisms are purposed to explain the antibacterial activity presented by AgNPs against gram-negative and gram-positive species, as represented in Figure 9. AgNPs size and shape allow them to have a high surface area to interact with the bacterial cell wall, providing interactions between the positive charge of the AgNPs and the negative charge present on bacteria' surface. Thus, the permeability of the bacterial wall is altered by AgNPs, with the formation of pores, that lead to the disruption of cell wall. Another mechanism purposed involves the transport of the AgNPs across the cell wall and release Ag^{+} ions. The release of these ions have a huge affinity to respiratory enzymes, proteins and DNA, causing protein denaturation, respiratory inhibition and DNA damage. Also, AgNPs can activate signal pathways that trigger the formation of ROS and cause cell apoptosis and inhibition of cell proliferation [72, 73, 75].

Therefore, the incorporation of AgNPs into electrospun membranes has been regarded as a possible strategy to improve their antibacterial performance. Chen and Chiang developed PU (7% w/w) nanofibers incorporating AgNPs (0.5% w/w), to produce an antimicrobial bioactive wound dressing [76]. The results obtained in their study revealed that the PU nanofibers incorporating AgNPs presented an antibacterial activity of 93.0 ± 2.4% and 84.0 ± 2.8%, against *S. aureus* and *E. coli*, respectively [76]. Furthermore, Augustine and their collaborators produced PCL membranes with AgNPs at different concentrations (0.05, 0.25, 0.5 and 1 wt%) [77]. The antibacterial activity of the

PCL/AgNPs nanocomposite membranes was analysed, through the disc diffusion method, against *E. coli* and *S. aureus*. The diameters of the inhibitory halos were 7.4 ± 0.3 mm and 6.2 ± 0.4 mm for PCL/0.05%AgNPs membrane, 7.6 ± 0.5 mm and 7.1 ± 0.3 mm for PCL/0.25%AgNPs membrane, 9.5 ± 0.6 mm and 7.4 ± 0.7 mm for PCL/0.5%AgNPs membrane, 11.6 ± 0.5 mm and 7.9 ± 0.6 mm for PCL/1%AgNPs membrane, against *S. aureus* and *E. coli*, respectively [77]. In another study, Rujitanaroj *et al.* also investigated the antibacterial activity of the AgNPs incorporated into Gel (22% w/v) electrospun membrane containing 2.5 wt% $AgNO_3$. The authors concluded that these materials had great antibacterial activity against *P. aeruginosa*, *S. aureus*, *E. coli*, and *methicillin-resistant S. aureus* [78].

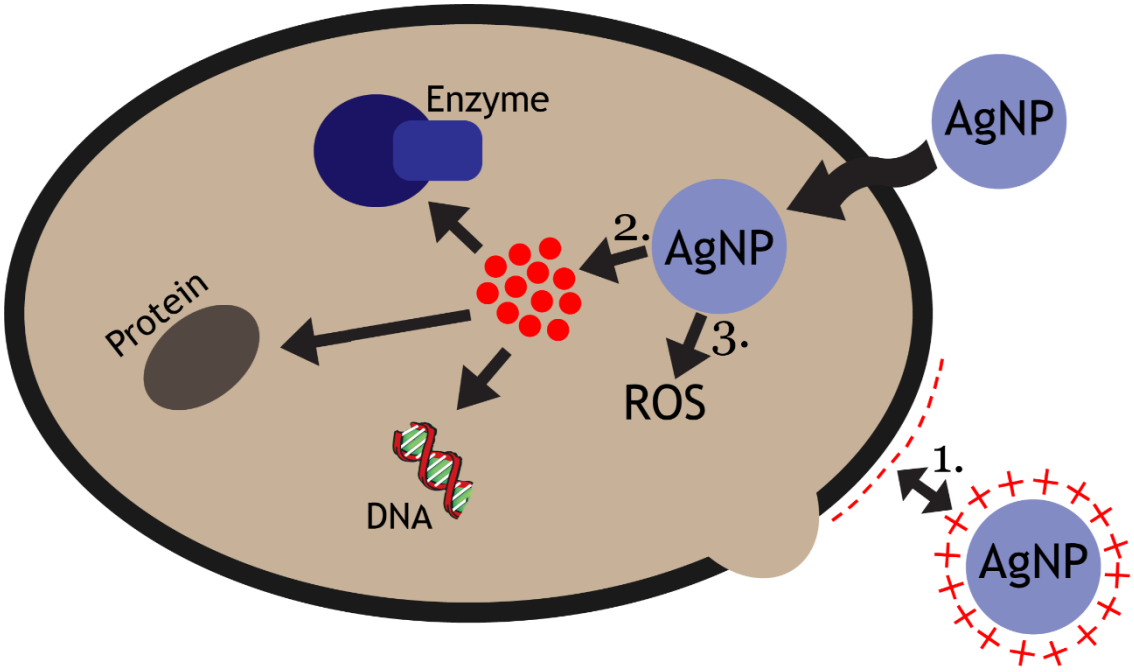

Figure 9. Illustration of the mechanisms proposed to explain the AgNPs bactericidal activity: 1. direct contact and consequent disruption; 2. capacity to cross the cell wall and release Ag^+ ions that have greater affinity to respiratory enzymes, proteins and DNA; 3. capacity to activate signal pathways that generate ROS.

1.6. Aims

The overall aim of the present Master dissertation work plan was to produce and characterize a new asymmetric electrospun membrane, aimed to improve the wound healing process.

The specific aims of this study were:

- Optimization and production of the top and bottom layers of the bilayered membrane (BM);
- Production of the BM;
- Synthesis and morphological/physicochemical characterization of the AgNPs;
- Evaluation and characterization of the physicochemical properties of the produced membranes;
- Evaluation and characterization of the biological properties of the produced membranes;
- Determination of antibacterial properties of the synthesized AgNPs.

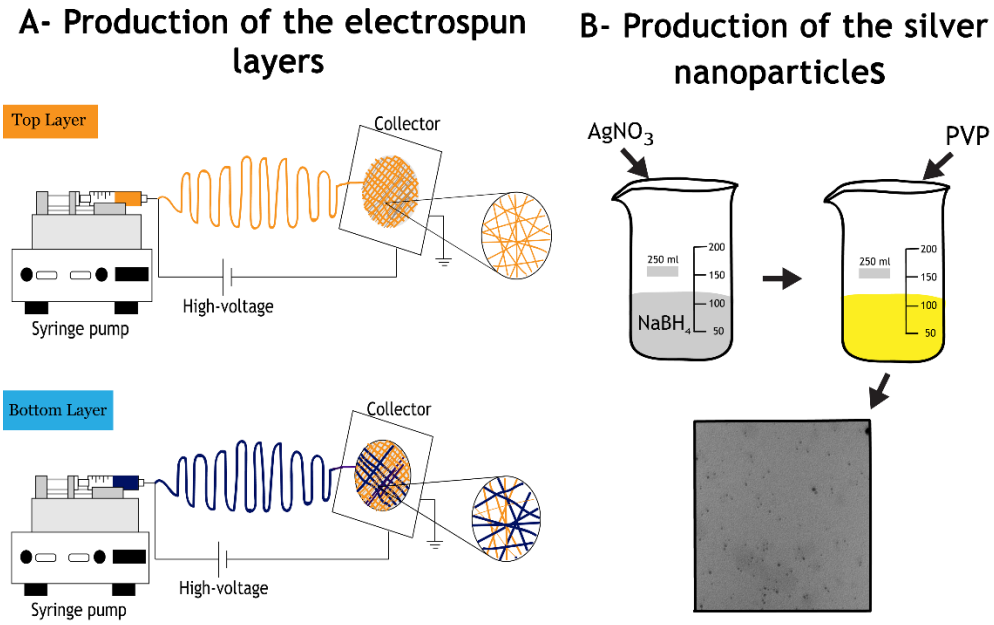

Figure 10. Schematic representation of the production of the electrospun membranes (PCL_CA, PVA_HA and BM), through the electrospinning technique (A) and production of the AgNPs through the reaction between $NaBH_4$ (reducing agent) with $AgNO_3$ (metal precursor), confirmed by the colour change to yellow, and the addition of polyvinylpyrrolidone (PVP) (metal stabilizers) (B).

Chapter II – Materials and Methods

2. Materials and methods

2.1. Materials

Trifluoroethanol was obtained by Acros organics (China). Hyaluronic acid (HA) extra low molecular weight (8000-15000 Da) was purchased from Carbosynth (Compton, UK). Fetal bovine serum (FBS) free from any antibiotic was bought from Biochrom AG (Berlin, Germany). Normal human dermal fibroblasts (NHDF) cells were acquired to PromoCell (Labclinics, S.A., Barcelona, Spain). 3-(4,5-dimethylthiazol- 2-yl)-5-(3-carboxymethoxyphenyl)-2 (4-sulfophenyl)-2H-tetrazolium (MTS) was obtained from Promega (Madison, WI, USA). Dulbecco's modified eagle's medium (DMEM-F12), Poly(ethylene oxide) (PEO) (Mw=300,000 g/mol), Poly(vinyl alcohol) (PVA) (Mw=85,000-124,000 g/mol) 99% hydrolyzed, Cellulose acetate (CA) (MW=30,000), Poly(caprolactone) (PCL) (MW=70,000-90,000), ethylenediaminetetraacetic acid (EDTA), sodium borohydride ($NaBH_4$), resazurin, glutaraldehyde, LB Broth, phosphate-buffered saline solution (PBS), Triton X-100 and trypsin were purchased from Sigma-Aldrich (Sintra, Portugal). Polyvinylpyrrolidone (PVP) (MW=44,000 g/mol) was acquired from BDH Chemicals Ltd. (Poole, UK). Silver nitrate ($AgNO_3$) was obtained from Honeywell (Charlotte, North Carolina, US). Tris Base and Quant-iT Pico Green dsDNA assay kit was supplied by ThermoFisher Scientific (Waltham, MA, USA). *Staphylococcus aureus* clinical isolate (*S. aureus*) ATCC 25923 and *Pseudomonas aeruginosa* (*P. aeruginosa*) obtained from a human sample, were used as models of prokaryotic organisms to evaluate the bactericidal activity exhibited by the silver nanoparticles produced. A Milli-Q Advantage A10 ultrapure Water Purification System (0.22 μm filtered; 18.2 MΩ/cm at 25 °C) was used to obtained double deionized and filtered water.

2.2. Methods

2.2.1. Production of the electrospun membranes

The production of the BM was performed by using two distinct polymeric solutions, which were electrospun using a conventional electrospinning apparatus, composed of a high voltage source (Spellman SL40*10, 0–40 kV; acquired to Spellman, Corporate Headquarters USA), a precision syringe pump (KDS-100), a plastic syringe with a stainless-steel needle (21 Gauge), and an aluminium foil connected to a copper collector. The top layer (PCL_CA) of the membrane was produced with a polymeric mixture of PCL (10% w/v) with CA (7% w/v) dissolved in trifluoroethanol solution (80% v/v). To

accomplish that, the solution was placed in the syringe and electrospun at a constant flow rate of 1.2 mL/h, using a distance of 15 cm to the collector and an applied voltage of 20kV.

Furthermore, the production of the bottom layer was accomplished through a combination of PVA (7% w/v), HA (20% w/v) and PEO (8% w/v). PEO was added to the mixture to obtain a solution with a suitable viscosity for the electrospinning process. This solution was electrospun on top of PCL_CA layer, at constant flow rate of 0.3 mL/h, using a working distance of 12 cm to the collector, and an applied voltage of 22kV, which allowed the production of PVA_HA membrane. The individual layers were also produced for comparative purposes.

2.2.2. Production of AgNPs

AgNPs were produced through the chemical reduction of silver, using $AgNO_3$ as a metal precursor and $NaBH_4$ as reducing agent, as previously described elsewhere [79, 80]. Initially, 5 mL of $AgNO_3$ solution (4 mM) were added dropwise to 30 mL of $NaBH_4$ solution (4 mM), under constant stirring at room temperature (RT), until an $AgNO_3$:$NaBH_4$ molar ratio of 1:5 was achieved. The nanoparticles synthesis was confirmed through the variation of colour in the solution, from colourless to yellow. Then, the solution was left under stirring for 30 min, and finally, 5 mL of 0.2% PVP solution (metal stabilizer) were added to the AgNPs solution. All procedures were performed in the dark in order to prevent any photodecomposition of $AgNO_3$.

2.2.2.1. Characterization of morphological and physicochemical properties of AgNPs

The AgNPs morphology was characterized through the transmission electron microscopy (TEM) by using a Hitachi–HT7700 microscope, operating with an accelerating voltage of 80 kV. The AgNPs samples were placed on a formvar-coated copper grid and dried at RT.

Furthermore, the hydrodynamic diameter and the zeta potential of the produced nanoparticles were determined through dynamic light scattering (DLS) analysis, by using a Zetasizer Nano ZS particle analyser (Malvern Instruments, Worcestershire, UK).

2.2.3. Attenuated total reflectance-Fourier transform infrared spectroscopy analysis

Attenuated total reflectance-Fourier transform infrared spectroscopy (ATR-FTIR) was used to characterize the chemical composition of the produced membranes and AgNPs. Their spectra and those of their raw materials were acquired using a Nicolet iS10 FTIR spectrophotometer (Thermo Scientific, Waltham, MA, USA), with an average of 128 scans, a spectral width between 4000 and 400 cm^{-1} and a spectral resolution of 32 cm^{-1}.

2.2.4. Characterization of the surface morphology of the produced membranes

Scanning electron microscopy (SEM) was used to characterize the surface morphology and the fiber's diameters distribution of the produced membranes [81]. To accomplish that, samples were mounted onto aluminium stubs using Araldite glue, and sputter-coated with gold using a Quorum Q150R ES sputter coater (Quorum Technologies Ltd., Laughton, East Sussex, UK). Then, SEM images were obtained using a Hitachi S-3400 N Scanning Electron Microscope (Hitachi, Tokyo, Japan), at an accelerating voltage of 20 kV. The average diameter of the nanofibers presented of the membranes was obtained by individual measurements (n=100) of nanofibers by using ImageJ software (Scion Corp., Frederick, MD).

2.2.5. Determination of the membranes' porosity

The total porosity of the produced membranes was determined by using liquid displacement method, as previously described by Figueira and collaborators [52]. For that, the samples (n=5) were weighed and immersed in absolute EtOH during 1h, and then reweighed. Subsequently, the membranes' porosity was determined through Equation (1):

$$Porosity\ (\%) = \frac{W_w - W_d}{D_{ethanol} * V_{membrane}} * 100 \quad (1)$$

where W_w and W_d are the wet and dry weights of the membrane, respectively. $D_{ethanol}$ represents the density of EtOH at RT, and $V_{membrane}$ is the volume of the wet membrane.

2.2.6. Water vapor transmission rate of the produced membranes

The WVTR through the membranes was determined as described elsewhere [81]. Briefly, the membranes (n=5) were used to seal the opening of a glass test tube (1.77 cm^2) containing 10 mL of ultrapure water, and then a parafilm tape was used to fix the membranes and prevent water losses. Finally, the membranes were incubated at 37°C, and at specific time points, the amount of evaporated water was measured. The WVTR was determined through the Equation (2):

$$WVTR = \frac{W_{loss}}{A} \quad (2)$$

where W_{loss} is the daily weight loss of water and A is the area of the tube opening.

2.2.7. Evaluation of the membranes' swelling capacity

The swelling capacity of the produced membranes was determined by immersing them in Tris hydrochloride (Tris-HCL) solution (pH=5 and pH=8), at 37°C, during 3 days under stirring (40 rpm) [81]. Then, at specific time points, the Tris-HCL was removed and the samples (n=5) were weighed. Finally, the swelling ratio was calculated through Equation (3):

$$Swelling\ ratio\ (Q) = \frac{W_t}{W_o} \quad (3)$$

where W_t is the weight of the membranes at time t and W_o is the initial weight of the membranes.

2.2.8. Characterization of the membranes' biodegradation profile

The degradation profile of the produced membranes was analysed by immersing them (n=5) in Tris-HCL (pH=5 and pH=8), under stirring (40 rpm), at 37°C [82]. The membranes were removed from the Tris-HCL, dried and weighed, after 1, 3 and 7 days. Finally, the weight loss percentage was calculated at each time point through the Equation (4):

$$Weight\ loss\ (\%) = \frac{W_i - W_t}{W_i} * 100\ (4)$$

where W_i corresponds to the initial weight of the sample and W_t to the weight of the sample at time t.

2.2.9. Characterization of the biological properties of the produced membranes

The biocompatibility of the membranes was characterized using an MTS assay, according to the ISO 10993-5:2009 (Biological evaluation of medical devices- Part 5: Tests for *in vitro* cytotoxicity), as previously described [82]. First, the produced membranes (n=5), with sizes inferior to 10% of the well area, were placed into 96-well plates and then sterilized under UV irradiation (254 nm, ≈7 mW cm^{-2}) for 1h. NHDF cells (used as model) were seeded in contact with membranes at a density of 10 × 10^3 cells/well and incubated at 37°C and 5% CO_2 humidified atmosphere. After 1, 3 and 7 days of incubation, the medium of each well was replaced by a mixture of 100 µL of fresh culture medium and 20 µL of MTS/phenazine methosulfate (PMS) reagent solution. Then, the plate was incubated for 4h, at 37°C, in a 5% CO_2 atmosphere and finally, the absorbance of each sample was measured at 490 nm using a microplate reader (Biorad xMark microplate spectrophotometer). Cells incubated with EtOH (70%) were used as positive control (K^+), while cells incubated only with culture medium were used as negative control (K^-).

Further, dsDNA quantification was performed in order to evaluate DNA integrity of NHDF cells in contact with the produced membranes. To accomplish that, a Quant-iT PicoGreen dsDNA Assay kit was used, following a protocol previously reported in literature [81, 82]. In brief, cells were initially seeded in contact with the membranes (n=5) and incubated for 1, 3 and 7 days. After each time point, 1mL of Triton X-100 (1x) was added to the wells to induce the cell lysis, during 1h. Then, the samples were placed into 1.5 mL Eppendorf tubes and exposed to a freeze-thaw cycle, sonicated and centrifuged at RT (14,000 g), for 15 min. After that, 100 µL of the supernatant were combined to an equal volume of PicoGreen solution (1:200 dilution of the PicoGreen reagent in TE Buffer (1x)), added to the samples and incubated for 10–15 min in the dark. Finally, the fluorescence was measured at excitation and emission wavelengths of 485 nm and 535 nm, respectively, using a microplate reader (Spectramax Gemini EM spectrofluorometer (Molecular Devices LLC, California, USA)). A calibration curve was determined with known concentrations of dsDNA and the obtained fluorescence values were used to calculate the dsDNA concentrations of each sample.

2.2.10. Characterization of the antibacterial properties of AgNPs

The AgNPs antibacterial activity was evaluated by using *S. aureus* and *P. aeruginosa* as a gram-positive and gram-negative bacteria model, respectively. To accomplish that, different concentrations of AgNPs (2–265 μg/mL) were placed in contact with the bacterial culture at density of 1 x 10^6 Colony-forming units (CFU)/mL. After 24h of incubation, the minimum inhibitory concentration (MIC) of AgNPs was determined, by using the resazurin assay as previously described elsewhere [79, 83]. For that purpose, 20 μL of resazurin (0.5 mg/mL) were added to 100 μL of each bacterial suspension, and a negative control (without AgNPs) and a positive control (containing Kanamycin antibiotic (30 mg/mL)) were also prepared. Then, the bacterial growth was quantified by the measurement of the fluorescence by using a fluorescence plate reader (Spectramax Gemini EM spectrofluorometer (Molecular Devices LLC, California, USA)) with filter set Ex_{560}/Em_{590}.

2.2.11. Statistical analysis

The statistical analysis of the obtained results was performed using one-way analysis of variance (ANOVA), with the Newman-Keuls post hoc test. A p value lower than 0.05 ($p < 0.05$) was considered statistically significant.

Chapter III - Results and Discussion

3. Results and discussion

3.1. Characterization of the produced membranes

3.1.1. Characterization of the morphology and composition of the produced membranes

In this study, an asymmetric membrane composed of a PCL_ CA top layer and a PVA_HA bottom layer was produced through electrospinning, aiming to mimic the epidermis and dermis of native skin, respectively.

The properties of electrospun asymmetric membrane produced herein were assessed through different techniques. ATR-FTIR analysis was performed to characterize both layers of the membrane, as well as the raw materials used in their production (see further details in Figure 11). The PCL_CA spectrum (Figure 11A) exhibits the characteristics peaks of PCL at 2940 cm^{-1} (CH_2 stretching), 1724 cm^{-1} (C=O stretching), and 1170 cm^{-1} (C-O-C stretching) [52]. In addition, the characteristic peaks of CA were also observed at 1731 cm^{-1} (C=O stretching), 1370 cm^{-1} (CH_3 stretching) and 1226 cm^{-1} (C-O-C stretching) [64]. Further, in the PVA_HA membrane spectrum the characteristic peaks of PVA at 3303 cm^{-1} (O-H stretching), 2883 cm^{-1} (CH_2 stretching), 1410 cm^{-1} (CH-O-H stretching), 1096 cm^{-1} (C-O stretching) and 838 cm^{-1} (C-C stretching) can be observed (Figure 11B) [82]. Moreover, the characteristic peaks of HA can also be visualized at 3294 cm^{-1} (OH and NH stretching), 1610 cm^{-1} (C=O stretching), 1399 cm^{-1} (C-O in combination with C=O) and 1035 cm^{-1} (C-O-C stretching) [52, 70]. The absorption peaks of PEO were noticed at 2876 cm^{-1} (CH_2 stretching) and 1090 cm^{-1} (C-O-C stretching) [84]. In general, the acquired spectra show that all materials used for membrane production exhibit their characteristic peaks.

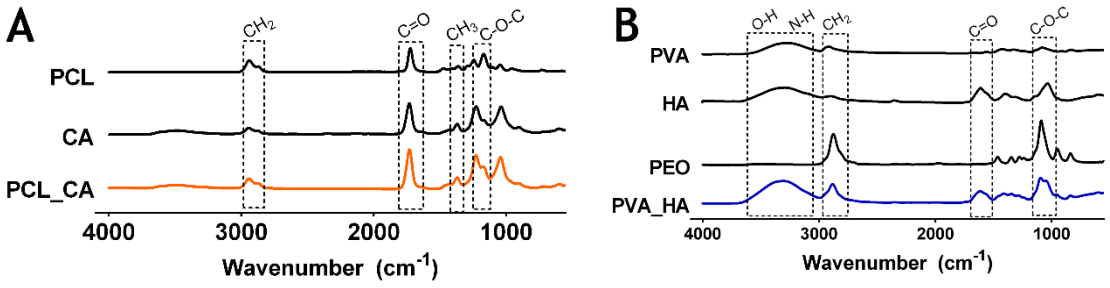

Figure 11. ATR-FTIR spectra of the PCL_CA membrane (A) and PVA_HA membrane (B) as well as their respective raw materials.

In turn, the morphology of the electrospun nanofibers was assessed by SEM analysis, and the fibers' diameter was measured with ImageJ software (Figure 12). The SEM

images showed that the produced membranes presented a 3D nanofiber mesh composed of continuous randomly oriented and non-beaded fibers. Moreover, the PCL_CA and PVA_HA membranes exhibited mean diameters of 615.12 ± 139.47 nm and 284.9 ± 117.17 nm, respectively. Such values are in concordance with other studies reported in the literature, since the higher fiber diameter values were also obtained for PCL (≈550 nm) and CA (593 nm) nanofibers [85, 86], whereas the average diameter reported for CS/PVA and SF/HA nanofibers were 313.61 ± 5.37 nm and 270.0 ± 82.2 nm, respectively [53, 87].

In addition, it is worth to notice that both produced layers presented nanofibers with diameters quite similar to those displayed by the collagen fibrils found in the ECM (50-500 nm), thus highlighting the structural similarity of the produced membrane with the native skin [41, 52, 82].

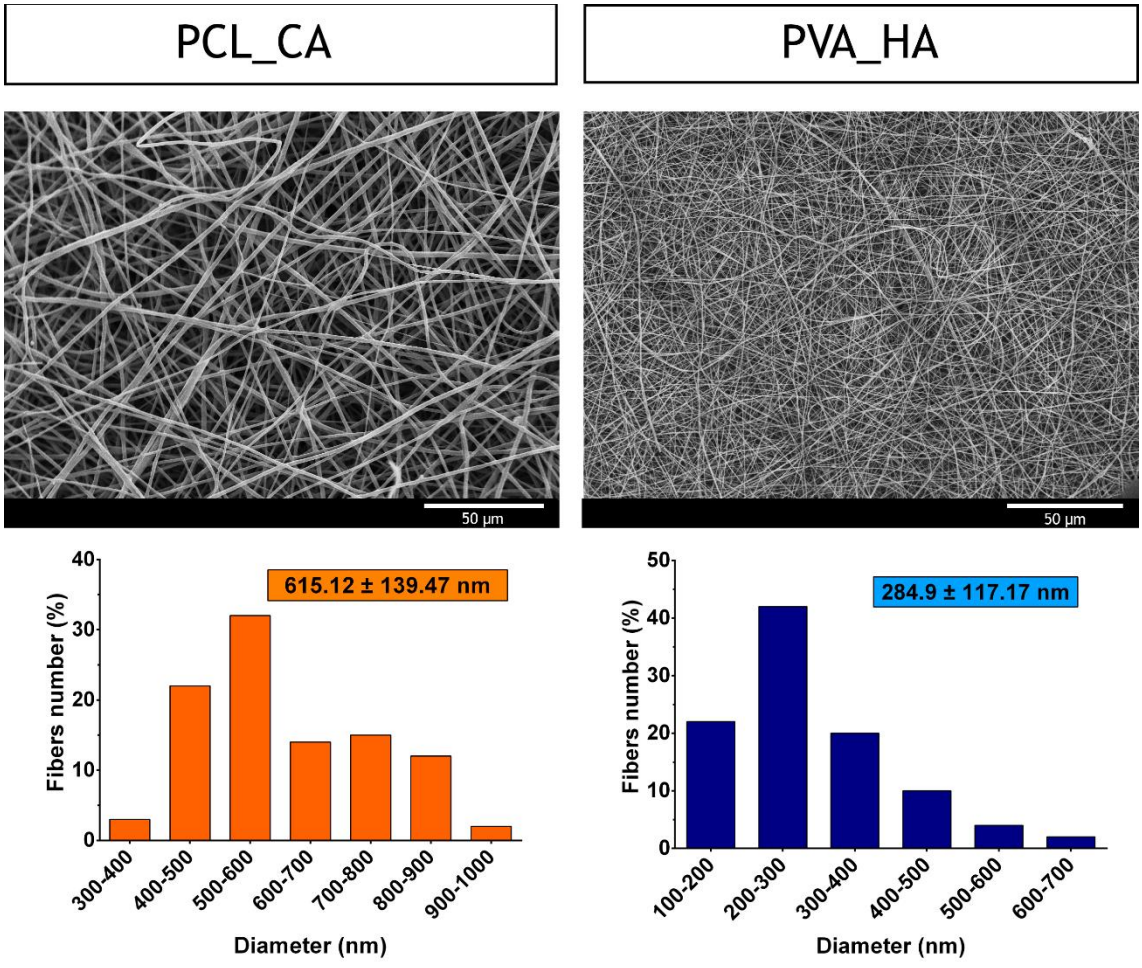

Figure 12. Characterization of the morphological properties of the produced electrospun membranes. SEM images and distribution of the fibers' diameters of the PCL_CA and PVA_HA membranes.

3.1.2. Evaluation of the total porosity of the produced membranes

The porosity of the membranes was determined through the fluid displacement method aiming to determine the percentage of void spaces available in membranes' structure. Such spaces are crucial to promote the gases and nutrients exchanges as well as the cell migration [88, 89]. The results presented in Figure 13A demonstrated that PCL_CA and PVA_HA membranes displayed porosity values of 81.41 ± 5.20% and 94.13 ± 18.92%, respectively. Moreover, the BM displayed a total porosity of 89.31 ± 7.48%.

The top layer (PCL_CA) presented a lower porosity value, which is crucial for preventing bacterial contamination [50, 52]. In fact, Mi *et al.* verified that the porosity values of 62.9%, 74.4%, 86.7%, 93.5% for CS membranes impaired the penetration of *P. aeruginosa* and *S. aureus* [90]. Besides, similar results were also reported by Chumpol *et al.* that produced an electrospun CA (7%) membrane with 77.3 ± 5.2% of porosity [91]. In contrast, the bottom layer (PVA_HA) exhibited a porosity value higher than 90%, which is considered appropriated for promoting the cell and nutrients infiltration [70]. Such differences on porosity values between top and bottom layers were already noticed by other researchers, where the top layer presented the lowest porosity (55 ± 5%), and the bottom layer had 97.8 ± 4.5% of porosity [92].

Moreover, the porosity values determined are compatible with the desired function that each layer will perform, *i.e.*, the non-porous top layer will avoid microorganism penetration whereas the highly porous bottom layer (≈90%) will allow cell adhesion, migration, and proliferation [89].

3.1.3. Characterization of the swelling profile of the produced membranes

During the healing process, the activity of the inflammatory cells (neutrophils, macrophages and platelets) results in the production of exudate. The exudate is a mixture of the electrolytes, glucose, cytokines, leukocytes, metalloproteinases, macrophages and microorganisms, which should not remain at wound site for long periods of time [93, 94]. In this way, an ideal wound dressing must be able to absorb the excessive exudate, in order to prevent the occurrence of skin maceration and infections [95]. Herein, the exudate absorption capacity of membranes was assessed through the determination of their swelling profile. For this purpose, the membranes were incubated in Tris-HCL at pH=5 and pH=8, to mimic the pH of healthy and injured skin, respectively (Figure 13B) [51, 53]. The data obtained reveal that the top, bottom layers and BM present swelling ratio values of 10.75 ± 1.32, 23.07 ± 2.52 and 41.80 ± 1.44 at pH=5 and 12.10 ± 0.77, 24.72 ± 1.28, and 39.11 ± 8.06, at pH=8, respectively.

The PCL_CA membrane had the lowest swelling ratio values (≈11), which is expectable since PCL and CA present the lowest content of hydroxyl groups, leading to a lower water solubility [62, 96]. Such low swelling capacity of the top layer will impair the microorganism growth, avoid the body dehydration as well as provide protection to the wound site [93]. The results obtained are in agreement with that previously published in literature, where it was noticed that when the concentration of CA increased, the swelling capacity of hydrogel decreased [97].

On the other hand, the PVA_HA membrane presents a high swelling capacity (≈24), that can be explained by the large number of carboxyl and hydroxyl groups available on PVA and HA polymers [20, 59, 98]. Similar results were previously reported by Miguel *et al.*, who obtained a higher swelling ratio (≈45) for the SF_HA_THY membranes [53]. In the same way, Gorska *et al.* noticed that PVA asymmetric membrane possessed a high capacity to absorb and retain water within its structure (swelling ≈70) [99].

The results obtained in these studies highlight the excellent ability of the PVA_HA membrane to remove the excess of exudate and provide a suitable environment for the wound healing process occur.

In turn, the combination of the top and bottom nanofibrous layers resulted in the production of a BM with a similar swelling profile to the bottom layer, revealing its capacity to prevent the occurrence of skin maceration and infections, as well as support cell migration, adhesion, proliferation and differentiation [88, 94].

3.1.4. Determination of the membranes' water vapor transmission rate

The WVTR is another feature that allow to evaluate the capacity of the membranes to provide a moist environment to the wound site [88, 89]. The obtained results demonstrated that the produced membranes present WVTR values of 2366.10 ± 69.36 mL/m²/day, 2164.97 ± 184.35 mL/m²/day and 2234.46 ± 21.33 mL/m²/day for the PCL_CA, PVA_HA and BM, respectively (as shown in Figure 13C). These results are within the ideal range recommended (2000–2500 mL/m²/day), revealing that the produced membranes are capable of providing a suitable environment for cell adhesion and proliferation. Such range is described as ideal since a high WVTR contributes for the dehydration of the wound and consequently to the dressing attachment, whereas a low WVTR can cause exudate retention, leading to skin maceration [95].

Further, the WVTR values displayed by the produced membranes are higher than those presented by commercial wound dressings and electrospun membranes already reported in the literature, as showed in Table 2 [100-102].

Table 2. Comparison of the water vapor transmission rate of different wound dressings reported in the literature and available in the market.

Wound dressing	**WVTR (g/m²/day)**	**Reference**
PCL/CS_Aloe Vera_PEO asymmetric Membrane	1252.35 ± 21.22	[92]
PCL_HA/CS_Zn electrospun bilayer membrane	1762.91 ± 187.50	[52]
CS_Arginine membrane	1713 ± 26	[101]
CS electrospun membranes	1353	[102]
PVA/CS membranes	214 ± 16	[51]
Tegasorb® (ConvaTec Ltd)	136 ± 15	[100]
Bioclusive® (Johnson-Johnson)	394 ± 12	[100]
Comfeel® (Coloplast A/S)	285 ± 8	[100]
Duoderm® (ConvaTec Ltd)	889 ± 49	[100]
IntraSite® (Smith & Nephew)	357 ± 29	[100]

3.1.5. Characterization of the biodegradation profile of the produced membranes

Nowadays, researchers from the tissue engineering area have been working to develop biodegradable wound dressings that display a degradation profile that is compatible with the rate of tissue regeneration. Such feature requires an appropriate selection of the materials used in the membrane production, since a high degradation rate impairs the mechanical support, whereas a lower degradation rate cause a stress shielding phenomena, hampering the healing process [37]. In this way, the degradation rate of the produced membranes was evaluated along 7 days of incubation in Tris-HCL at pH=5 and pH=8 (Figure 13D). The results obtained show that the PCL_CA membrane had a weight loss of 14.02 ± 1.18 % and 12.46 ± 6.16 %, the PVA_HA lost 61.37 ± 6.53 % and 65.42 ± 1.92 %, and the BM presented a weight loss of 45.76 ± 11.34 % and 50.93 ± 6.99 %, at pH=5 and pH=8, respectively.

The lower degradation values exhibited by the top layer can be explained by the weak interaction of the PCL and CA with water molecules. The top layer degradation only occurs as a consequence of the hydrolytic cleavage of ester groups of PCL and/or hydrolysis, de-acetylization/enzymatic degradation of hydroxyl and acetyl groups of CA [96, 103]. Indeed, the high stability exhibited by PCL and CA in water was already noticed in other works. Nosar *et al.* obtained a weight loss of 16.50 % for CA membranes immersed in DMEM supplemented with 10 % (v/v) FBS (pH 7.4), for 30 days [104]. On the other hand, Hivechi *et al.* noticed that PCL nanofibers incorporating cellulose nanocrystals presented a weight loss value < 10%, after 7 days in PBS [105].

Contrarily, the bottom layer exhibited a higher weight loss due to the presence of hydrophilic polymers in its composition, *i.e.*, PVA and HA. These may suffer degradation through the hydrolysis of their hydroxyl groups [98, 106]. In fact, their easy interaction with water have been widely reported in the literature [107]. For example, Tamahkar *et al.* obtained weight loss values of ≈50%, after 8 days, for PVA, HA and Gel hydrogels [107].

The BM produced herein presented a more controlled degradation profile, *i.e.*, had higher values of weight loss than the top layer, however not so high as the bottom layer, thus providing a provisional matrix for cell adhesion and proliferation at a controlled rate.

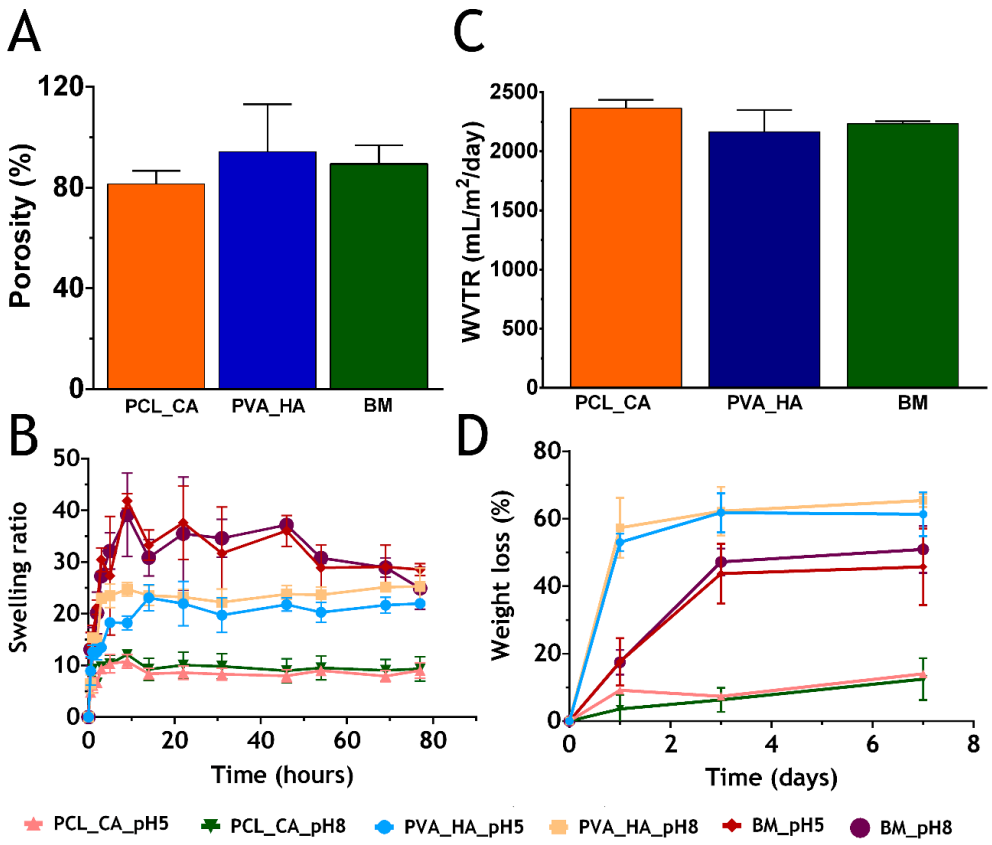

Figure 13. Characterization of physicochemical properties of the produced membranes. Determination of the electrospun membranes' porosity (A); Characterization of the membranes' swelling profile, at pH=5 and pH=8 (B); Determination of the WVTR value of the membranes (C); Characterization of the membranes' weight loss at pH=5 and pH=8 (D).

3.1.6. Characterization of biological properties of the produced membranes

The biological features of the produced membranes were evaluated through optical microscopy, MTS and dsDNA quantification assays, using NHDF as model cells. NHDF were chosen due to its essential role in production of ECM proteins, such as collagen,

elastin, fibrin, and fibronectin, that are enrolled in the formation of the granulation tissue, angiogenesis, and consequently, in the re-establishment of skin structure and functions [27]. To accomplish the characterization of the biological properties of the produced membranes, NHDF cells were seeded in contact with the produced membranes and then optical microscopic images were acquired (Figure 14) to characterize cells' morphology in contact with the membranes. The images obtained show that the NHDF cells exhibited an elongated morphology like those cells present in the negative control (*i.e.,* cells incubated just with culture medium), while in the positive control the cells displayed a spherical shape (characteristic of dead cells). In addition, the results of the MTS assay, demonstrated that NHDF cells remained viable over a period of 7 days in contact with the produced membranes (Figure 15A). Such results suggest that the PCL_CA and PVA_HA membranes did not induce any cytotoxic effect on fibroblast cells. Further, the results of the dsDNA quantification corroborate the MTS results, evidencing that no significant differences were noticed in DNA content of cells incubated with the produced membranes, over a period of 7 days (Figure 15B). All data obtained confirms the excellent biocompatible profile of the PCL_CA and PVA_HA membranes, and its ability to promote the proliferation of fibroblast cells, emphasizing its potential for improving the wound healing process.

Indeed, the biocompatibility of the polymers used in the production of the membranes (PCL, CA, PVA and HA) was previously reported by other authors [104, 108]. Nosar *et al.* observed that CA electrospun membranes with different concentrations (4% to 14%) did not induce any cytotoxic effect on the L929 cells [104]. In turn, Li *et al.* verified that the presence of HA within PCL/SF/HA nanofibrous membranes improves the cellular infiltration and proliferation [108]. Furthermore, it has been also described that HA interacts with CD44 receptors available in skin cells, thus regulating the re-epithelization process, guiding the fibroblasts invasion and proliferation, as well as promoting its differentiation into myofibroblasts, which contributes to the wound contraction [67, 69, 109].

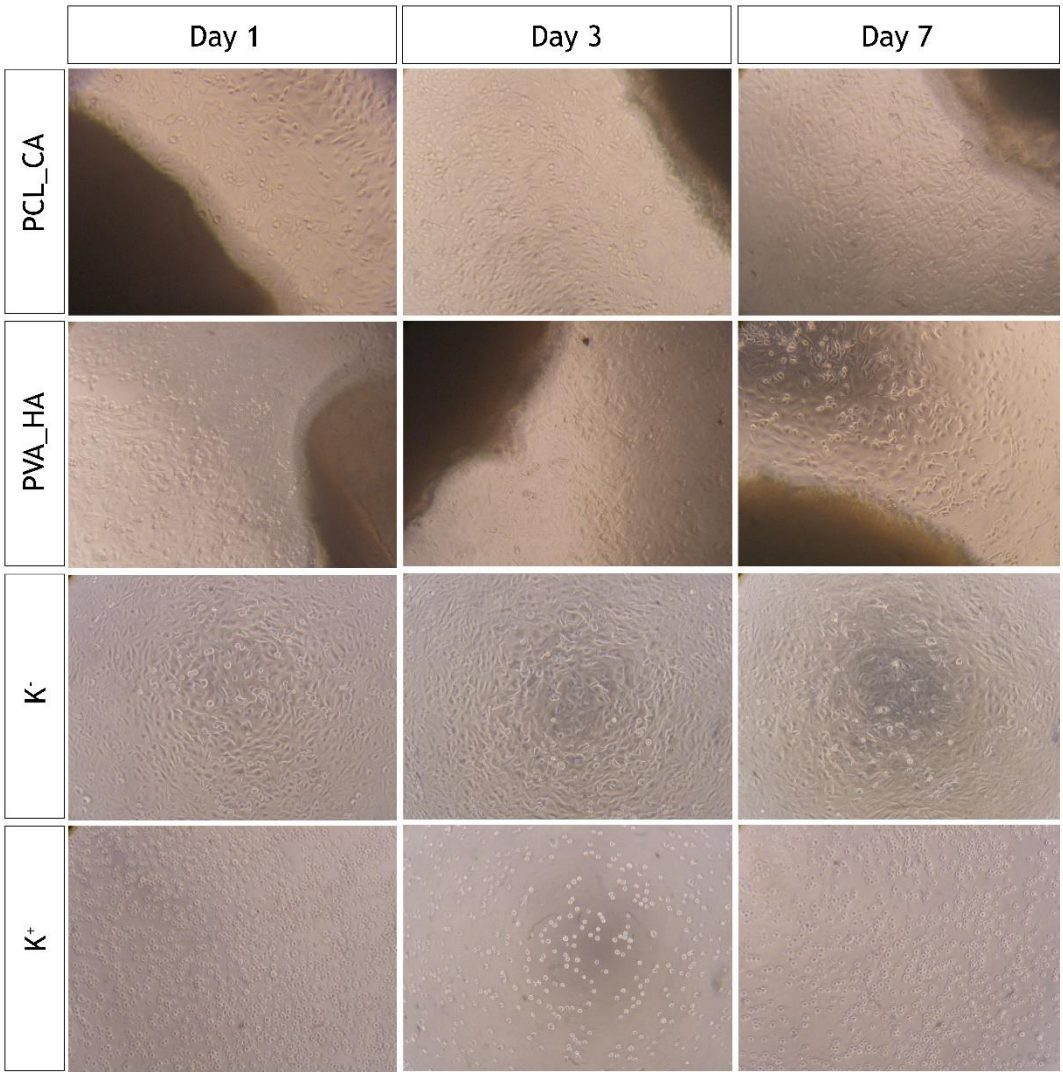

Figure 14. Optical microscopic images of NHDF cells cultured in contact with the produced membranes (PCL_CA and PVA_HA) after 1, 3, and 7 days of incubation; K^- (negative control); K^+ (positive control).

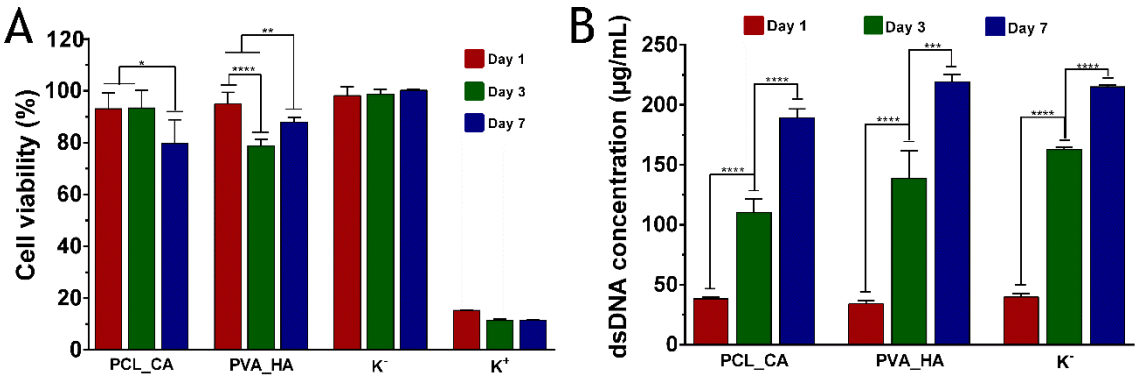

Figure 15. Characterization of the nanofibrous membranes' biocompatibility. Evaluation of NHDF cells viability when cultured in the presence of the produced electrospun membranes after 1, 3 and 7 days of incubation, through MTS analysis (A) and dsDNA assay (B). K^- (live cells); K^+ (dead cells). Data are presented as the mean ± standard deviation, n = 5, *p< 0.05, **p< 0.01, ***p< 0.001 and ****p< 0.0001.

3.2. Characterization of AgNPs

AgNPs were produced herein through the chemical reduction of silver, using $AgNO_3$ as a metal precursor, $NaBH_4$ as reducing agent and PVP as metal stabilizer, in order to avoid the agglomeration of the produced nanoparticles. After its synthesis, FTIR, UV–Vis, TEM and DLS analysis were performed to characterize AgNPs morphological and physicochemical properties (Figure 16). The FTIR spectrum of PVP (Figure 16A) displays the characteristic peaks at 2946 cm^{-1} (CH_2 stretching), 1278 cm^{-1} (C–N stretching) and 1648 cm^{-1} (C=O stretching). In the $AgNO_3$ spectrum, a major peak at 1279 cm^{-1} (characteristic of the ion pair $Ag^+NO_3^-$) is observed. Further, the characteristic peak of $AgNO_3$ is not visible in the AgNPs spectrum, which means that the reduction of the ion pair $AgNO_3$ occurs [79, 83].

Moreover, the UV-Vis spectra (Figure 16B) exhibited a characteristic extinction band at 400 nm, which indicates the presence of quasi-spherical AgNPs [79]. Further, the TEM image (Figure 16C) demonstrate that the AgNPs were successfully produced and presented the quasi-spherical shape. These properties ensure a high surface-to-volume ratio that is essential for its antimicrobial activity [110]. Moreover, the size and the zeta potential of the AgNPs were also determined through DLS analysis (Figure 16D). The produced AgNPs presented an average size of 24.05 ± 0.364 nm, values that are within the range size usually reported for this type of nanoparticles [79]. Moreover, a zeta potential of the AgNPs of -29.5 ± 6.9 mV was obtained.

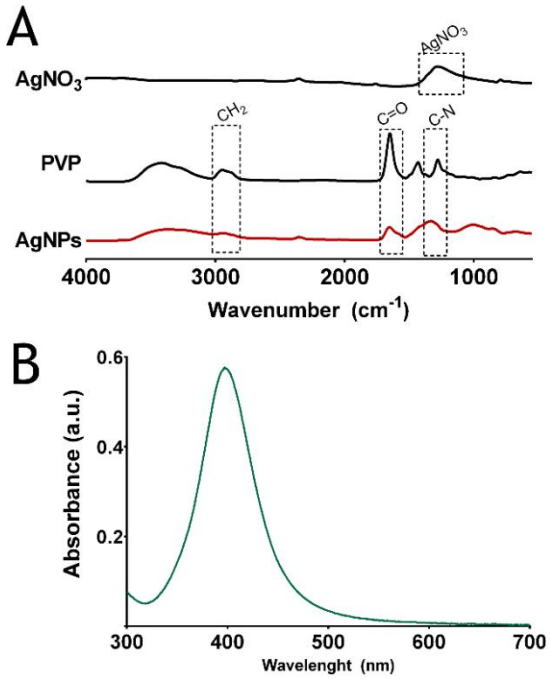

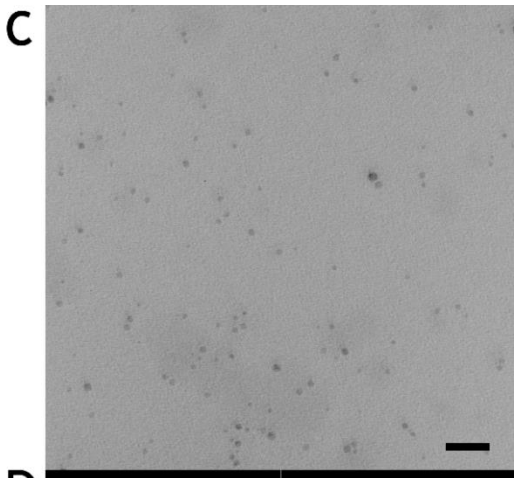

D

DLS analysis	AgNPs
Average size	24.05 ± 0.364 nm
Zeta potential	-29.5 ± 6.9 mV

Figure 16. Characterization of AgNPs. ATR-FTIR analysis (A), UV-Vis spectra (B), TEM analysis of the AgNPs at 80x (the scale bar represents 100 nm) (C) and DLS analysis (D).

3.2.1. Antibacterial properties of AgNPs

The AgNPs were produced to be incorporated within PVA_HA nanofibers in order to confer it antibacterial properties. The antibacterial properties of the AgNPs were evaluated against *P. aeruginosa* and *S. aureus*, that were used as a gram-negative and a gram-positive bacteria model, respectively, since they are usually associated with skin infections [73]. To accomplish that, *P. aeruginosa* and *S. aureus* were incubated with different concentrations of AgNPs (2-265 μg/mL), during 24h at 37 °C. The obtained results (Figure 17) showed that for concentrations of AgNPs higher than 30 μg/mL the bacterial growth was avoided. Such antibacterial effect may be explained by the capacity of AgNPs to cross the bacteria cell wall, and consequent Ag^+ release and ROS production, which leads to the impaired bacterial growth [72].

Further, the results obtained in this study are in agreement with that obtained by Bhatia *et al.*, who produced PVP coated AgNPs with a charge of -39.86 mV, and attained antibacterial properties against gram-positive bacteria (*Bacillus subtilis, S. aureus, Streptococcus mutans, Streptococcus pyogenes*) and gram-negative bacteria (*E. coli, P. aeruginosa, Pseudomonas fluorescens*). Further, the authors also determinated the MIC values, using different concentrations of AgNPs (375, 187.5, 93.75, 46.85, and 23.45 μg/mL), and a MIC value of 46 μg/mL was determined against *E. coli*, *S. aureus*, *Bacillus subtilis* and *P. aeruginosa* [111]. In the same way, Singh *et al.* also produced AgNPs with a zeta potential of -22.4 ± 2.1 mV and antibacterial activity against *P. aeruginosa, E. coli, Vibrio parahaemolyticus* and *S. aureus* [112].

Furthermore, the results also showed that AgNPs produced herein exhibited a higher antibacterial activity against *P. aeruginosa* than *S. aureus*. This can be explained by the differences found on cell wall structure of gram-negative and gram-positive bacteria, *i.e.*, the gram-negative *P. aeruginosa* presents a thinner cell wall that propelled the penetration of silver nanoparticles into the cell wall [113]. In the future, AgNPs will be incorporated into the bottom layer of the asymmetric membrane, in order to confer it antibacterial properties, which are essential to avoid the occurrence of skin infections.

Until now, the incorporation of AgNPs into PVA_HA nanofibers was already tested through the blend and physical adsorption techniques. However, both strategies have not yet allowed the incorporation of the nanoparticles. To accomplish the incorporation of AgNPs within the nanofibrous mesh, AgNPs concentration will be optimized and other incorporation methodology will be tried.

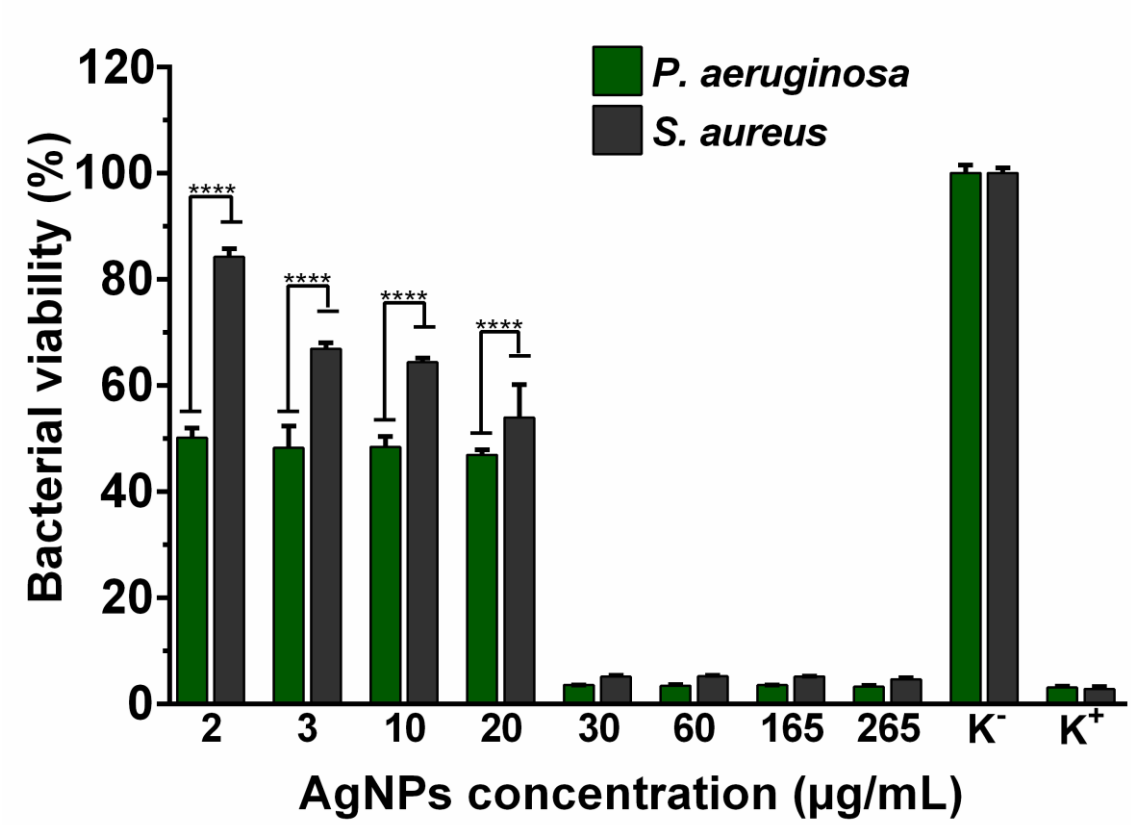

Figure 17. Determination of MIC values of the produced AgNPs, after 24h in contact with *S. aureus* and *P. aeruginosa* (K^- (live bacteria); K^+ (death bacteria)). Data are presented as the mean ± standard deviation, n = 5, ****p < 0.0001.

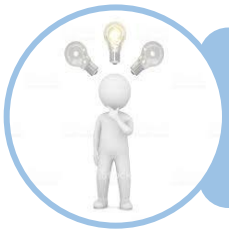

Chapter IV - Conclusions and Future Perspectives

4. Conclusions and Future Perspectives

Acute and chronic skin injuries continue to be a major health issue for the worldwide population. The therapeutic strategies used up to now in the clinic still present some limitations, and none of them is capable of fully restoring the structure and functions of the native skin. Nevertheless, bioactive dressings such as electrospun membranes have captured the attention of researchers, due to its capacity to mimic the morphology and structure of the ECM of the skin, as well as allow the incorporation of antibacterial agents within their structure. Further, the versatility of the electrospinning technique enable the combination of different polymers, thus promoting the production of layers with distinct features. In this way, tissue engineering researchers have been used this technique to developed different asymmetric membranes that mimic both layers of skin.

Herein, an asymmetric electrospun membrane was produced and characterized to mimic the epidermis and dermis layers. In this way, the top layer manufactured with PCL_ CA which was conceived to reproduce the epidermis features, presented a lower porosity and swelling capacity, features that are essential to provide a protective barrier against external harmful agents. Unlike, the bottom layer, composed of PVA_ HA mimicked the dermis, displayed a higher porosity and swelling ability, properties that are fundamental for wound exudate absorption, maintenance of a moist environment, and an enhanced diffusion of nutrients, cells and bioactive molecules. Furthermore, the AgNPs were also produced aiming to incorporate them within the BM membrane, to confer it antimicrobial properties. Although, due to experimental constrains this task was not accomplished.

Overall, the results obtained in the present dissertation work demonstrated that the produced bilayer membrane (PCL_CA/PVA_HA) has suitable properties to be used as a wound dressing for skin regeneration.

In addition, the incorporation of the produced AgNPs and/or another antimicrobial molecules into bottom layer will confer it antimicrobial activity, which is essential to avoid the skin infections. Furthermore, the incorporation of other bioactive molecules (*e.g.* vitamins, proteins or GF) can be also be envisioned in order to augment the biological performance of the asymmetric wound dressings. Moreover, *in vivo* assays may also be performed to further evaluate the therapeutic potential of the electrospun bilayer membrane in the healing process. On the other side, the incorporation of biosensors into nanofibers could be also hypothesized to allow the real-time monitorization of the wound bed environment parameters (like pH or temperature).

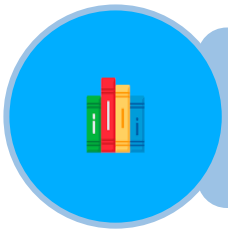

Chapter V - References

5. References

1. Guerra, A., J. Belinha, and R.N. Jorge, *Modelling skin wound healing angiogenesis: A review*. Journal of theoretical biology, 2018. **459**: p. 1-17.
2. Wong, R., S. Geyer, W. Weninger, J.C. Guimberteau, and J.K. Wong, *The dynamic anatomy and patterning of skin*. Experimental dermatology, 2016. **25**(2): p. 92-98.
3. Rezvani Ghomi, E., S. Khalili, S. Nouri Khorasani, R. Esmaeely Neisiany, and S. Ramakrishna, *Wound dressings: Current advances and future directions*. Journal of Applied Polymer Science, 2019. **136**(27): p. 47738.
4. Juráňová, J., J. Franková, and J. Ulrichová, *The role of keratinocytes in inflammation*. Journal of Applied Biomedicine, 2017. **15**(3): p. 169-179.
5. Zhang, Z. and B.B. Michniak-Kohn, *Tissue engineered human skin equivalents*. Pharmaceutics, 2012. **4**(1): p. 26-41.
6. Losquadro, W.D., *Anatomy of the skin and the pathogenesis of nonmelanoma skin cancer*. Facial Plastic Surgery Clinics, 2017. **25**(3): p. 283-289.
7. Vig, K., A. Chaudhari, S. Tripathi, S. Dixit, R. Sahu, S. Pillai, V.A. Dennis, and S.R. Singh, *Advances in skin regeneration using tissue engineering*. International journal of molecular sciences, 2017. **18**(4): p. 789.
8. Sainio, A. and H. Järveläinen, *Extracellular matrix-cell interactions: Focus on therapeutic applications*. Cellular signalling, 2020. **66**: p. 109487.
9. Lai-Cheong, J.E. and J.A. McGrath, *Structure and function of skin, hair and nails*. Medicine, 2013. **41**(6): p. 317-320.
10. Dekoninck, S. and C. Blanpain, *Stem cell dynamics, migration and plasticity during wound healing*. Nature cell biology, 2019. **21**(1): p. 18-24.
11. Vary Jr, J.C., *Selected disorders of skin appendages--acne, alopecia, hyperhidrosis*. The Medical Clinics of North America, 2016. **99**(6): p. 1195-211.
12. Kolarsick, P.A., M.A. Kolarsick, and C. Goodwin, *Anatomy and physiology of the skin*. Journal of the Dermatology Nurses' Association, 2011. **3**(4): p. 203-213.
13. Byrd, A.L., Y. Belkaid, and J.A. Segre, *The human skin microbiome*. Nature Reviews Microbiology, 2018. **16**(3): p. 143.
14. Zahedi, P., I. Rezaeian, S.O. Ranaei-Siadat, S.H. Jafari, and P. Supaphol, *A review on wound dressings with an emphasis on electrospun nanofibrous polymeric bandages*. Polymers for Advanced Technologies, 2010. **21**(2): p. 77-95.
15. Rezaie, F., M. Momeni-Moghaddam, and H. Naderi-Meshkin, *Regeneration and repair of skin wounds: various strategies for treatment*. The international journal of lower extremity wounds, 2019. **18**(3): p. 247-261.

16. Rittié, L., *Cellular mechanisms of skin repair in humans and other mammals.* Journal of cell communication and signaling, 2016. **10**(2): p. 103-120.
17. Ambekar, R.S. and B. Kandasubramanian, *Advancements in nanofibers for wound dressing: A review*. European Polymer Journal, 2019. **117**: p. 304-336
18. Boateng, J. and O. Catanzano, *Advanced therapeutic dressings for effective wound healing—a review*. Journal of pharmaceutical sciences, 2015. **104**(11): p. 3653-3680.
19. Dreifke, M.B., A.A. Jayasuriya, and A.C. Jayasuriya, *Current wound healing procedures and potential care.* Materials Science and Engineering: C, 2015. **48**: p. 651-662.
20. Wang, J. and M. Windbergs, *Functional electrospun fibers for the treatment of human skin wounds.* European Journal of Pharmaceutics and Biopharmaceutics, 2017. **119**: p. 283-299.
21. Boateng, J.S., K.H. Matthews, H.N. Stevens, and G.M. Eccleston, *Wound healing dressings and drug delivery systems: a review*. Journal of pharmaceutical sciences, 2008. **97**(8): p. 2892-2923.
22. Morton, L.M. and T.J. Phillips, *Wound healing and treating wounds: differential diagnosis and evaluation of chronic wounds.* Journal of the American Academy of Dermatology, 2016. **74**(4): p. 589-605.
23. Zhao, N., X. Wang, L. Qin, M. Zhai, J. Yuan, J. Chen, and D. Li, *Effect of hyaluronic acid in bone formation and its applications in dentistry*. Journal of biomedical materials research Part A, 2016. **104**(6): p. 1560-1569.
24. Shah, S.A., M. Sohail, S. Khan, M.U. Minhas, M. de Matas, V. Sikstone, Z. Hussain, M. Abbasi, and M. Kousar, *Biopolymer-based biomaterials for accelerated diabetic wound healing: A critical review*. International journal of biological macromolecules, 2019. **139**: p. 975-993.
25. Singh, S., A. Young, and C.-E. McNaught, *The physiology of wound healing*. Surgery (Oxford), 2017. **35**(9): p. 473-477.
26. Gonzalez, A.C.d.O., T.F. Costa, Z.d.A. Andrade, and A.R.A.P. Medrado, *Wound healing-A literature review*. Anais brasileiros de dermatologia, 2016. **91**(5): p. 614-620.
27. Das, S. and A.B. Baker, *Biomaterials and nanotherapeutics for enhancing skin wound healing*. Frontiers in bioengineering and biotechnology, 2016. **4**: p. 82.
28. Haddad, A.G., G. Giatsidis, D.P. Orgill, and E.G. Halvorson, *Skin substitutes and bioscaffolds: temporary and permanent coverage.* Clinics in plastic surgery, 2017. **44**(3): p. 627-634.

29. Xue, M., R. Zhao, H. Lin, and C. Jackson, *Delivery systems of current biologicals for the treatment of chronic cutaneous wounds and severe burns*. Advanced drug delivery reviews, 2018. **129**: p. 219-241.
30. Nyame, T.T., H.A. Chiang, T. Leavitt, M. Ozambela, and D.P. Orgill, *Tissue-engineered skin substitutes*. Plastic and reconstructive surgery, 2015. **136**(6): p. 1379-1388.
31. Adibfar, A., H. Retrouvey, S. Padeanu, M.G. Jeschke, and S. Shahrokhi, *Current State of Selected Wound Regeneration Templates and Temporary Covers*. Current Trauma Reports, 2019. **5**(2): p. 79-89.
32. Dai, C., S. Shih, and A. Khachemoune, *Skin substitutes for acute and chronic wound healing: an updated review*. Journal of Dermatological Treatment, 2020. p. 1-31.
33. Felgueiras, H.P. and M.T.P. Amorim, *Functionalization of electrospun polymeric wound dressings with antimicrobial peptides*. Colloids and Surfaces B: Biointerfaces, 2017. **156**: p. 133-148.
34. Dhivya, S., V.V. Padma, and E. Santhini, *Wound dressings–a review*. BioMedicine, 2015. **5**(4): p. 22.
35. Dias, J., P. Granja, and P. Bártolo, *Advances in electrospun skin substitutes*. Progress in Materials Science, 2016. **84**: p. 314-334.
36. Goodarzi, P., K. Falahzadeh, M. Nematizadeh, P. Farazandeh, M. Payab, B. Larijani, A.T. Beik, and B. Arjmand, *Tissue engineered skin substitutes*, in *Cell Biology and Translational Medicine, Volume 3*. 2018, Springer. p. 143-188.
37. Fahimirad, S. and F. Ajalloueian, *Naturally-derived electrospun wound dressings for target delivery of bio-active agents*. International journal of pharmaceutics, 2019. **566**: p. 307-328.
38. Lu, B., T. Wang, Z. Li, F. Dai, L. Lv, F. Tang, K. Yu, J. Liu, and G. Lan, *Healing of skin wounds with a chitosan–gelatin sponge loaded with tannins and platelet-rich plasma*. International journal of biological macromolecules, 2016. **82**: p. 884-891.
39. Zhang, X., X. Kang, L. Jin, J. Bai, W. Liu, and Z. Wang, *Stimulation of wound healing using bioinspired hydrogels with basic fibroblast growth factor (bFGF)*. International journal of nanomedicine, 2018. **13**: p. 3897-3906.
40. Tang, K.-C., K.-C. Yang, C.-W. Lin, Y.-K. Chen, T.-Y. Lu, H.-Y. Chen, N.-C. Cheng, and J. Yu, *Human adipose-derived stem cell secreted extracellular matrix incorporated into electrospun poly (lactic-co-glycolic acid) nanofibrous dressing for enhancing wound healing*. Polymers, 2019. **11**(10): p. 1609.

41. Miguel, S.P., D.R. Figueira, D. Simões, M.P. Ribeiro, P. Coutinho, P. Ferreira, and I.J. Correia, *Electrospun polymeric nanofibres as wound dressings: A review*. Colloids and surfaces B: Biointerfaces, 2018. **169**: p. 60-71.
42. Jones, V., J.E. Grey, and K.G. Harding, *Wound dressings*. Bmj, 2006. **332**(7544): p. 777-780.
43. Preem, L. and K. Kogermann, *Electrospun Antimicrobial Wound Dressings: Novel Strategies to Fight Against Wound Infections*. Recent Clinical Techniques, Results, and Research in Wounds. 2018, Springer. p. 1-41.
44. Weller, C. and G. Sussman, *Wound dressings update*. Journal of pharmacy practice and research, 2006. **36**(4): p. 318-324.
45. Lionelli, G.T. and W.T. Lawrence, *Wound dressings*. Surgical Clinics, 2003. **83**(3): p. 617-638.
46. Coelho, D.S., B. Veleirinho, T. Alberti, A. Maestri, R. Yunes, P.F. Dias, and M. Maraschin, *Electrospinning Technology: Designing Nanofibers toward Wound Healing Application*, in *Nanomaterials-Toxicity, Human Health and Environment*. 2018, IntechOpen.
47. Norouzi, M., S.M. Boroujeni, N. Omidvarkordshouli, and M. Soleimani, *Advances in skin regeneration: application of electrospun scaffolds*. Advanced healthcare materials, 2015. **4**(8): p. 1114-1133.
48. Liu, Y., S. Zhou, Y. Gao, and Y. Zhai, *Electrospun nanofibers as a wound dressing for treating diabetic foot ulcer*. Asian Journal of Pharmaceutical Sciences, 2019. **14**(2): p. 130-143.
49. Haider, A., S. Haider, and I.-K. Kang, *A comprehensive review summarizing the effect of electrospinning parameters and potential applications of nanofibers in biomedical and biotechnology*. Arabian Journal of Chemistry, 2018. **11**(8): p. 1165-1188.
50. Miguel, S.P., A.F. Moreira, and I.J. Correia, *Chitosan based-asymmetric membranes for wound healing: A review*. International journal of biological macromolecules, 2019. **127**: p. 460-475.
51. Morgado, P.I., P.F. Lisboa, M.P. Ribeiro, S.P. Miguel, P.C. Simões, I.J. Correia, and A. Aguiar-Ricardo, *Poly (vinyl alcohol)/chitosan asymmetrical membranes: Highly controlled morphology toward the ideal wound dressing*. Journal of membrane science, 2014. **469**: p. 262-271.
52. Figueira, D.R., S.P. Miguel, K.D. de Sá, and I.J. Correia, *Production and characterization of polycaprolactone-hyaluronic acid/chitosan-zein electrospun bilayer nanofibrous membrane for tissue regeneration*. International journal of biological macromolecules, 2016. **93**: p. 1100-1110.

53. Miguel, S.P., D. Simões, A.F. Moreira, R.S. Sequeira, and I.J. Correia, *Production and characterization of electrospun silk fibroin based asymmetric membranes for wound dressing applications*. International journal of biological macromolecules, 2019. **121**: p. 524-535.
54. Chen, S.-H., Y. Chang, K.-R. Lee, and J.-Y. Lai, *A three-dimensional dual-layer nano/microfibrous structure of electrospun chitosan/poly (d, l-lactide) membrane for the improvement of cytocompatibility*. Journal of membrane science, 2014. **450**: p. 224-234.
55. Janmohammadi, M. and M. Nourbakhsh, *Electrospun polycaprolactone scaffolds for tissue engineering: a review*. International Journal of Polymeric Materials and Polymeric Biomaterials, 2019. **68**(9): p. 527-539.
56. Mondal, D., M. Griffith, and S.S. Venkatraman, *Polycaprolactone-based biomaterials for tissue engineering and drug delivery: Current scenario and challenges*. International Journal of Polymeric Materials and Polymeric Biomaterials, 2016. **65**(5): p. 255-265.
57. Suwantong, O., *Biomedical applications of electrospun polycaprolactone fiber mats*. Polymers for Advanced Technologies, 2016. **27**(10): p. 1264-1273.
58. Adeli-Sardou, M., M.M. Yaghoobi, M. Torkzadeh-Mahani, and M. Dodel, *Controlled release of lawsone from polycaprolactone/gelatin electrospun nano fibers for skin tissue regeneration*. International journal of biological macromolecules, 2019. **124**: p. 478-491.
59. Aytimur, A., S. Koçyiğit, İ. Uslu, and F. Gökmeşe, *Preparation and characterization of polyvinyl alcohol based copolymers as wound dressing fibers*. International Journal of Polymeric Materials and Polymeric Biomaterials, 2015. **64**(3): p. 111-116.
60. Safaee-Ardakani, M.R., A. Hatamian-Zarmi, S.M. Sadat, Z.B. Mokhtari-Hosseini, B. Ebrahimi-Hosseinzadeh, J. Rashidiani, and H. Kooshki, *Electrospun Schizophyllan/polyvinyl alcohol blend nanofibrous scaffold as potential wound healing*. International journal of biological macromolecules, 2019. **127**: p. 27-38.
61. Ganesh, M., A.S. Aziz, U. Ubaidulla, P. Hemalatha, A. Saravanakumar, R. Ravikumar, M.M. Peng, E.Y. Choi, and H.T. Jang, *Sulfanilamide and silver nanoparticles-loaded polyvinyl alcohol-chitosan composite electrospun nanofibers: synthesis and evaluation on synergism in wound healing*. Journal of Industrial and Engineering Chemistry, 2016. **39**: p. 127-135.
62. Suwantong, O. and P. Supaphol, *Applications of cellulose acetate nanofiber mats*, in *Handbook of Polymer Nanocomposites. Processing, Performance and Application*. 2015, Springer. p. 355-368.

63. Khoshnevisan, K., H. Maleki, H. Samadian, S. Shahsavari, M.H. Sarrafzadeh, B. Larijani, F.A. Dorkoosh, V. Haghpanah, and M.R. Khorramizadeh, *Cellulose acetate electrospun nanofibers for drug delivery systems: Applications and recent advances*. Carbohydrate polymers, 2018. **198**: p. 131-141.
64. Vatankhah, E., M.P. Prabhakaran, G. Jin, L.G. Mobarakeh, and S. Ramakrishna, *Development of nanofibrous cellulose acetate/gelatin skin substitutes for variety wound treatment applications*. Journal of biomaterials applications, 2014. **28**(6): p. 909-921.
65. Samadian, H., M. Salehi, S. Farzamfar, A. Vaez, A. Ehterami, H. Sahrapeyma, A. Goodarzi, and S. Ghorbani, *In vitro and in vivo evaluation of electrospun cellulose acetate/gelatin/hydroxyapatite nanocomposite mats for wound dressing applications*. Artificial cells, nanomedicine, and biotechnology, 2018. **46**(sup1): p. 964-974.
66. Knopf-Marques, H., M. Pravda, L. Wolfova, V. Velebny, P. Schaaf, N.E. Vrana, and P. Lavalle, *Hyaluronic acid and its derivatives in coating and delivery systems: applications in tissue engineering, regenerative medicine and immunomodulation*. Advanced healthcare materials, 2016. **5**(22): p. 2841-2855.
67. Graça, M.F., S.P. Miguel, C.S. Cabral, and I.J. Correia, *Hyaluronic acid-based wound dressings: a review*. Carbohydrate Polymers, 2020. **241**: p. 116364.
68. Chen, W.J., *Functions of hyaluronan in wound repair*, in *Hyaluronan*. 2002, Elsevier. p. 147-156.
69. Aya, K.L. and R. Stern, *Hyaluronan in wound healing: rediscovering a major player*. Wound repair and regeneration, 2014. **22**(5): p. 579-593.
70. Chanda, A., J. Adhikari, A. Ghosh, S.R. Chowdhury, S. Thomas, P. Datta, and P. Saha, *Electrospun chitosan/polycaprolactone-hyaluronic acid bilayered scaffold for potential wound healing applications*. International journal of biological macromolecules, 2018. **116**: p. 774-785.
71. Shin, Y.C., D.M. Shin, E.J. Lee, J.H. Lee, J.E. Kim, S.H. Song, D.Y. Hwang, J.J. Lee, B. Kim, and D. Lim, *Hyaluronic acid/PLGA core/shell fiber matrices loaded with EGCG beneficial to diabetic wound healing*. Advanced healthcare materials, 2016. **5**(23): p. 3035-3045.
72. Miguel, S.P., R.S. Sequeira, A.F. Moreira, C.C. Cabral, A.G. Mendonça, P. Ferreira, and I.J. Correia, *An overview of electrospun membranes loaded with bioactive molecules for improving the wound healing process*. European Journal of Pharmaceutics and Biopharmaceutics, 2019. **139**: p. 1-22.

73. Simões, D., S.P. Miguel, M.P. Ribeiro, and P. Coutinho, *European Journal of Pharmaceutics and Biopharmaceutics Recent advances on antimicrobial wound dressing: A review*. 2018. **127**: p. 130-141.
74. Zhang, X.-F., Z.-G. Liu, W. Shen, and S. Gurunathan, *Silver nanoparticles: synthesis, characterization, properties, applications, and therapeutic approaches*. International journal of molecular sciences, 2016. **17**(9): p. 1534.
75. Srikar, S.K., D.D. Giri, D.B. Pal, P.K. Mishra, and S.N. Upadhyay, *Green synthesis of silver nanoparticles: a review*. Green and Sustainable Chemistry, 2016. **6**(01): p. 34.
76. Chen, J.-P. and Y. Chiang, *Bioactive electrospun silver nanoparticles-containing polyurethane nanofibers as wound dressings*. Journal of nanoscience and nanotechnology, 2010. **10**(11): p. 7560-7564.
77. Augustine, R., N. Kalarikkal, and S. Thomas, *Electrospun PCL membranes incorporated with biosynthesized silver nanoparticles as antibacterial wound dressings*. Applied Nanoscience, 2016. **6**(3): p. 337-344.
78. Rujitanaroj, P.-o., N. Pimpha, and P. Supaphol, *Wound-dressing materials with antibacterial activity from electrospun gelatin fiber mats containing silver nanoparticles*. Polymer, 2008. **49**(21): p. 4723-4732.
79. Silva, E., S.M. Saraiva, S.P. Miguel, and I.J. Correia, *PVP-coated silver nanoparticles showing antifungal improved activity against dermatophytes*. Journal of nanoparticle research, 2014. **16**(11): p. 2726.
80. De Sá, K.D., D.R. Figueira, S.P. Miguel, T.R. Correia, A.P. Silva, and I.J. Correia, *3D scaffolds coated with nanofibers displaying bactericidal activity for bone tissue applications*. International Journal of Polymeric Materials and Polymeric Biomaterials, 2017. **66**(9): p. 432-442.
81. Simões, D., S.P. Miguel, and I.J. Correia, *Biofunctionalization of electrospun poly (caprolactone) fibers with Maillard reaction products for wound dressing applications*. Reactive and Functional Polymers, 2018. **131**: p. 191-202.
82. Sequeira, R.S., S.P. Miguel, C.S. Cabral, A.F. Moreira, P. Ferreira, and I.J. Correia, *Development of a poly (vinyl alcohol)/lysine electrospun membrane-based drug delivery system for improved skin regeneration*. International journal of pharmaceutics, 2019. **570**: p. 118640.
83. Correia, T.R., D.R. Figueira, K.D. de Sá, S.P. Miguel, R.G. Fradique, A.G. Mendonça, and I.J. Correia, *3D printed scaffolds with bactericidal activity aimed for bone tissue regeneration*. International journal of biological macromolecules, 2016. **93**: p. 1432-1445.

84. Chen, G., J. Guo, J. Nie, and G. Ma, *Preparation, characterization, and application of PEO/HA core shell nanofibers based on electric field induced phase separation during electrospinning*. Polymer, 2016. **83**: p. 12-19.
85. Ren, K., Y. Wang, T. Sun, W. Yue, and H. Zhang, *Electrospun PCL/gelatin composite nanofiber structures for effective guided bone regeneration membranes*. Materials Science and Engineering: C, 2017. **78**: p. 324-332.
86. Quirós, J., S. Gonzalo, B. Jalvo, K. Boltes, J.A. Perdigón-Melón, and R. Rosal, *Electrospun cellulose acetate composites containing supported metal nanoparticles for antifungal membranes*. Science of The Total Environment, 2016. **563-564**: p. 912-920.
87. Ahmed, R., M. Tariq, I. Ali, R. Asghar, P.N. Khanam, R. Augustine, and A. Hasan, *Novel electrospun chitosan/polyvinyl alcohol/zinc oxide nanofibrous mats with antibacterial and antioxidant properties for diabetic wound healing*. International journal of biological macromolecules, 2018. **120**: p. 385-393.
88. Jin, G., M.P. Prabhakaran, D. Kai, S.K. Annamalai, K.D. Arunachalam, and S. Ramakrishna, *Tissue engineered plant extracts as nanofibrous wound dressing*. Biomaterials, 2013. **34**(3): p. 724-734.
89. Rasouli, R., A. Barhoum, M. Bechelany, and A. Dufresne, *Nanofibers for biomedical and healthcare applications*. Macromolecular bioscience, 2019. **19**(2): p. 1800256.
90. Mi, F.-L., S.-S. Shyu, Y.-B. Wu, S.-T. Lee, J.-Y. Shyong, and R.-N. Huang, *Fabrication and characterization of a sponge-like asymmetric chitosan membrane as a wound dressing*. Biomaterials, 2001. **22**(2): p. 165-173.
91. Chumpol, J. and S. Siri, *Electrospun cellulose acetate membrane for size separating and antibacterial screening of crude polysaccharides*. IET nanobiotechnology, 2016. **10**(6): p. 405-410.
92. Miguel, S.P., M.P. Ribeiro, P. Coutinho, and I.J. Correia, *Electrospun polycaprolactone/aloe vera_chitosan nanofibrous asymmetric membranes aimed for wound healing applications*. Polymers, 2017. **9**(5): p. 183.
93. Derakhshandeh, H., S.S. Kashaf, F. Aghabaglou, I.O. Ghanavati, and A. Tamayol, *Smart bandages: the future of wound care*. Trends in biotechnology, 2018. **36**(12): p. 1259-1274.
94. Adderley, U.J., *Managing wound exudate and promoting healing*. British journal of community nursing, 2010. **15**(Sup1): p. S15-S20.
95. Morgado, P.I., A. Aguiar-Ricardo, and I.J. Correia, *Asymmetric membranes as ideal wound dressings: An overview on production methods, structure,*

properties and performance relationship. Journal of Membrane Science, 2015. **490**: p. 139-151.

96. Siddiqui, N., S. Asawa, B. Birru, R. Baadhe, and S. Rao, *PCL-based composite scaffold matrices for tissue engineering applications*. Molecular biotechnology, 2018. **60**(7): p. 506-532.
97. Muñoz-García, R.O., M.E. Hernández, G.G. Ortiz, V.V. Fernández, M.R. Arellano, and J.C. Sánchez-Díaz, *A novel polyacrylamide-based hydrogel crosslinked with cellulose acetate and prepared by precipitation polymerization*. Química Nova, 2015. **38**(8): p. 1031-1036.
98. Fallacara, A., E. Baldini, S. Manfredini, and S. Vertuani, *Hyaluronic acid in the third millennium*. Polymers, 2018. **10**(7): p. 701.
99. Górska, A., P. Dorożyński, W.P. Węglarz, K. Jasiński, M. Kurek, R. Jachowicz, J. Klaja, and P. Kulinowski, *Spatiotemporal characterization of hydration process of asymmetric polymeric wound dressings for decubitus ulcers*. Journal of Biomedical Materials Research Part B: Applied Biomaterials, 2018. **106**(2): p. 843-853.
100. Wu, P., A. Fisher, P. Foo, D. Queen, and J. Gaylor, *In vitro assessment of water vapour transmission of synthetic wound dressings*. Biomaterials, 1995. **16**(3): p. 171-175.
101. Antunes, B.P., A.F. Moreira, V. Gaspar, and I. Correia, *Chitosan/arginine–chitosan polymer blends for assembly of nanofibrous membranes for wound regeneration*. Carbohydrate polymers, 2015. **130**: p. 104-112.
102. Naseri, N., C. Algan, V. Jacobs, M. John, K. Oksman, and A.P. Mathew, *Electrospun chitosan-based nanocomposite mats reinforced with chitin nanocrystals for wound dressing*. Carbohydrate polymers, 2014. **109**: p. 7-15.
103. Entcheva, E., H. Bien, L. Yin, C.-Y. Chung, M. Farrell, and Y. Kostov, *Functional cardiac cell constructs on cellulose-based scaffolding*. Biomaterials, 2004. **25**(26): p. 5753-5762.
104. Nosar, M.N., M. Salehi, S. Ghorbani, S.P. Beiranvand, A. Goodarzi, and M. Azami, *Characterization of wet-electrospun cellulose acetate based 3-dimensional scaffolds for skin tissue engineering applications: influence of cellulose acetate concentration*. Cellulose, 2016. **23**(5): p. 3239-3248.
105. Hivechi, A., S.H. Bahrami, and R.A. Siegel, *Drug release and biodegradability of electrospun cellulose nanocrystal reinforced polycaprolactone*. Materials Science and Engineering: C, 2019. **94**: p. 929-937.
106. Chiellini, E., A. Corti, S. D'Antone, and R. Solaro, *Biodegradation of poly (vinyl alcohol) based materials*. Progress in Polymer Science, 2003. **28**(6): p. 963-1014.

107. Tamahkar, E., B. Özkahraman, A.K. Süloğlu, N. İdil, and I. Perçin, *A novel multilayer hydrogel wound dressing for antibiotic release*. Journal of Drug Delivery Science and Technology, 2020. **58**: p. 101536.
108. Li, L., Y. Qian, C. Jiang, Y. Lv, W. Liu, L. Zhong, K. Cai, S. Li, and L. Yang, *The use of hyaluronan to regulate protein adsorption and cell infiltration in nanofibrous scaffolds*. Biomaterials, 2012. **33**(12): p. 3428-3445.
109. Webber, J., R.H. Jenkins, S. Meran, A. Phillips, and R. Steadman, *Modulation of TGFβ1-dependent myofibroblast differentiation by hyaluronan*. The American journal of pathology, 2009. **175**(1): p. 148-160.
110. Bryaskova, R., D. Pencheva, S. Nikolov, and T. Kantardjiev, *Synthesis and comparative study on the antimicrobial activity of hybrid materials based on silver nanoparticles (AgNps) stabilized by polyvinylpyrrolidone (PVP)*. Journal of chemical biology, 2011. **4**(4): p. 185.
111. Bhatia, D., A. Mittal, and D.K. Malik, *Antimicrobial activity of PVP coated silver nanoparticles synthesized by Lysinibacillus varians*. 3 Biotech, 2016. **6**(2): p. 196.
112. Singh, H., J. Du, P. Singh, and T.H. Yi, *Ecofriendly synthesis of silver and gold nanoparticles by Euphrasia officinalis leaf extract and its biomedical applications*. Artificial cells, nanomedicine, and biotechnology, 2018. **46**(6): p. 1163-1170.
113. Durán, N., M. Durán, M.B. De Jesus, A.B. Seabra, W.J. Fávaro, and G. Nakazato, *Silver nanoparticles: A new view on mechanistic aspects on antimicrobial activity*. Nanomedicine: Nanotechnology, Biology and Medicine, 2016. **12**(3): p. 789-799.